



HAL
open science

Influences of propylene/propyne addition on toluene pyrolysis in a single-pulse shock tube

Wenyu Sun, Alaa Hamadi, Said Abid, Nabiha Chaumeix, Andrea Comandini

► **To cite this version:**

Wenyu Sun, Alaa Hamadi, Said Abid, Nabiha Chaumeix, Andrea Comandini. Influences of propylene/propyne addition on toluene pyrolysis in a single-pulse shock tube. *Combustion and Flame*, 2022, 236, pp.111799. 10.1016/j.combustflame.2021.111799 . hal-03408293

HAL Id: hal-03408293

<https://hal.science/hal-03408293>

Submitted on 29 Oct 2021

HAL is a multi-disciplinary open access archive for the deposit and dissemination of scientific research documents, whether they are published or not. The documents may come from teaching and research institutions in France or abroad, or from public or private research centers.

L'archive ouverte pluridisciplinaire **HAL**, est destinée au dépôt et à la diffusion de documents scientifiques de niveau recherche, publiés ou non, émanant des établissements d'enseignement et de recherche français ou étrangers, des laboratoires publics ou privés.



Influences of propylene/propyne addition on toluene pyrolysis in a single-pulse shock tube

Wenyu Sun^{a,*}, Alaa Hamadi^a, Said Abid^{a,b}, Nabih Chaumeix^a, Andrea Comandini^{a,*}

^a CNRS-INSIS, I.C.A.R.E., 1C, Avenue de la recherche scientifique, 45071 Orléans cedex 2, France

^b Université d'Orléans, 6 Avenue du Parc Floral, 45100 Orléans, France



ARTICLE INFO

Article history:

Received 21 April 2021

Revised 13 September 2021

Accepted 14 September 2021

Keywords:

Toluene

Propylene

Propyne

Pyrolysis

Single-pulse shock tube

ABSTRACT

To explore the potential interactions between toluene/benzyl and the common C_3 combustion intermediates, toluene-propylene and toluene-propyne co-pyrolysis is studied in the current work by taking neat toluene pyrolysis as a reference. Experiments are carried out at a nominal pressure of 20 bar over a temperature range of 1050–1700 K, using a single-pulse shock tube facility coupled to the gas chromatography-mass spectrometry speciation diagnostic technique. Temperature-dependent mole fraction profiles are obtained for numerous species ranging from small-molecule products to three-ring polycyclic aromatic hydrocarbons (PAHs). A kinetic model, which has been under development in our serial works, is extended by including the interplays between toluene/benzyl and propylene/propyne chemistry. The updated model can satisfactorily predict the measurements, regarding the absolute mole fractions as well as the variation trends brought by different initial fuel compositions. Increased reactivity is observed in the conversion of toluene with the presence of propylene or propyne, while the consumption rates of the studied C_3 fuels are barely influenced by toluene. Benzene formation is facilitated by the C_3+C_3 reactions introduced by the C_3 fuels. The pyrolysis of propylene (or propyne) significantly enhances the level of C_1-C_3 molecules/radicals that further react with aromatic species. For instance, the reactions of benzyl+propyne result in much higher mole fractions and lower speciation temperature windows of indene and naphthalene in toluene-propylene (or propyne) co-pyrolysis. The reactions with small hydrocarbons result in reduced levels of benzyl and other C_7 radicals in the reaction system in toluene-propylene (or propyne) co-pyrolysis. Consequently, for the PAHs which are mainly formed through C_7+C_7 reactions, such as bibenzyl and phenanthrene, the mole fractions are lowered by the addition of propylene (or propyne). Propyne has more obvious influences on the species pool of toluene pyrolysis than propylene, because the effective C_7-C_3 interactions are mostly through the reactions between toluene/benzyl and propyne/propargyl in both cases of toluene-propylene and toluene-propyne co-pyrolysis.

© 2021 The Author(s). Published by Elsevier Inc. on behalf of The Combustion Institute.

This is an open access article under the CC BY license (<http://creativecommons.org/licenses/by/4.0/>)

1. Introduction

Towards a predictive kinetic model for the formation of polycyclic aromatic hydrocarbons (PAHs) in the combustion of practical and surrogate fuels, a good characterization of toluene/benzyl chemistry is an indispensable building block. Toluene/benzyl is produced as an active intermediate in the break-down of specific fuel components such as alkylbenzenes, and also acts as a starting precursor of large PAHs up to soot. To highlight the reaction channels from fuel dissociation to the formation of PAHs, toluene pyrolysis kinetics has been long pursued [1–12] under a wide range

of temperature/pressure conditions by means of experiments, theoretical calculations and detailed kinetic modeling. Benzyl is established as the most important product from the initial consumption steps of toluene. Owing to the resonance-stabilized nature, benzyl has been experimentally observed of relatively high concentrations [8,11], compared to other essential aromatic radicals such as phenyl. The fate of benzyl plays a fundamental role in controlling the system reactivity and the speciation of various aromatic products. Given such importance, the reaction scheme of benzyl decomposition has been extensively studied [13–18] and revisited even nowadays [19]. Nevertheless, besides dissociation to smaller molecules, benzyl also reacts with other species present in the reaction system, leading to mass growth. The radical-radical recombination reactions of benzyl and alkyl radicals, which are essentially the reverse processes of the benzylic C–C bond fission in

* Corresponding authors.

E-mail addresses: wenyu.sun@cnrs-orleans.fr (W. Sun), andrea.comandini@cnrs-orleans.fr (A. Comandini).

alkylbenzenes, lead to lengthening of the side chain on the aromatic ring. Benzyl+acetylene is found as an important source of indene formation, more efficient than the C_6+C_3 channels, on the C_9H_9 reaction potential energy surface [20,21]. Indane is observed in toluene-ethylene co-pyrolysis in our recent work [22], indicating the occurrence of ring-closure via benzyl-ethylene interaction. Similar to the first aromatic ring formation through allyl+propargyl recombination, benzyl+propargyl recombination is deemed as an important pathway leading to the second ring, i.e. naphthalene, after losing two H atoms [4,23,24]. The recombination of benzyl+phenyl and the subsequent dehydrogenation were included in kinetic models [10–12] to account for the formation of fluorene. Besides, the reaction between benzyl and o-benzyne was also found as a source of fluorene [25]. Sinha and coauthors studied the reactions starting from benzyl self-recombination [26] and benzyl+indenyl recombination [27], and pointed out that such pathways can efficiently lead to fused three- and four- ring aromatics under specific conditions.

Interactions between toluene/benzyl and C_2 fuels (acetylene and ethylene) are highlighted through investigating toluene- C_2 co-pyrolysis in our previous work [22]. Enhanced fuel decomposition reactivity and changed PAH speciation behaviors were observed when C_2 fuels were added to toluene pyrolysis. C_3 species are also ubiquitous in combustion reaction systems. Particularly, the resonance-stabilized radicals allyl and propargyl are established as important benzene precursors. In our recent work [28] mole fraction profiles of various species up to four ring PAHs were probed from propylene and propyne pyrolysis. Kinetic modeling analyses suggested that the build-up of PAHs in C_3 fuel pyrolysis largely depends on the reaction channels starting from benzene/phenyl [28]. It is worth exploring the potential interactions between toluene and C_3 fuels, which is scarcely addressed in literature [24], even though specific C_3 species, such as propyne and propargyl, are present among the species pool of toluene pyrolysis [11,12].

Therefore, in this work, we carry out shock tube pyrolysis experiments using argon diluted mixtures containing 100 ppm toluene, with or without 500 ppm propylene/propyne at a nominal pressure of 20 bar over a temperature range of 1050–1700 K. Post-shock gas mixtures are sampled for chemical composition analyses, yielding temperature-dependent mole fraction profiles for species ranging from small hydrocarbons to three-ring PAHs. Updates are made to an ongoing PAH formation kinetic model that has been developed in our recent works [12,22,28–30], mainly by supplementing cross-linkage reactions of toluene/benzyl and C_3 species. The joint experimental and kinetic modeling efforts are made to seek for answers to two major questions: 1. How will propylene and propyne influence the decomposition reactivity of toluene. More specifically, whether the “synergistic effects” observed in the toluene- C_2 co-pyrolysis [22,31] are also valid in the case of toluene and propylene (or propyne); 2. How will the added C_3 fuels influence the speciation behaviors, particularly for the aromatic species. Also, the responsible reaction processes will be identified and the differences of propylene and propyne addition will be unraveled.

2. Shock tube experiments

The pyrolysis experiments of neat toluene and toluene/propylene (or propyne) mixtures are carried out using the single-pulse shock tube facility at ICARE, CNRS, Orléans. The detailed descriptions about the shock tube and the coupled sampling GC/GC-MS speciation measuring system are well documented in our previous publications [12,22,29,30]. In brief, the driven section (78 mm in inner diameter and 6.0 m in length) of the shock tube is separated from the driver section by a double diaphragm section. To run the shock tube in a single-pulse fashion,

a dump tank, with a volume five times larger than the driven section, is placed near the diaphragm on the driven section side. The driven section is heated up at 90 °C and pumped to below 10^{-5} mbar using a molecular turbo pump before every experiment. Four pressure sensors (CHIMIE METAL A25L05B) are mounted on the side wall of the driven section at an interval of 150 mm, with the last one being 82 mm away from the end wall of the shock tube. The sensors record the time when the shock wave passes for the calculation of the incident shock velocity, which is further used to determine the post-shock conditions T_5 and p_5 by solving the conservation equations together with the ideal gas law and variable heat capacity ratio. The physical dimension of the shock detectors introduces uncertainties in the correlation between the time when the pressure rise is observed and the corresponding location on the sensitive area of the sensors. The sensitive areas extend around ± 1 mm with respect to the center of the sensor, thus the maximum error in the distance between two adjacent sensors is 2 mm. The presence of shock wave attenuation (below 2.5% for most experiments) can affect the correct estimate of the temperature since the withdrawn sample has an average composition that spans a relatively large volume. Given all the mentioned factors, an uncertainty of ± 30 K is estimated in the calculated T_5 . A PCB Piezotronics pressure sensor shielded by a layer of room-temperature vulcanizing (RTV) silicone is placed on the endwall to record the local pressure time. A typical endwall pressure profile as well as the corresponding definition of reaction time is shown in Fig. S1 in the Supplementary Material. The reaction time is specified as the time between the arrival of the shock wave and the point when the pressure drops to 80% p_5 , and it has a nominal value of 4.0 ms with the current experimental configuration. An air actuated valve is mounted at the center of the endwall, and its operation is triggered by the endwall pressure signal, with a delay set at 4.0 ms (equal to the nominal reaction time). The opening and closing of the sampling valve last hundreds of milliseconds, extracting a relatively large quantity of post-shock gas samples, so that trace PAH species can be detected and measured. The samples are transferred through SilcoTek tubes, which are heated up at 250 °C to minimize the loss of heavy species due to condensation. The chemical compositions of the samples are analyzed by two GCs placed in series. The first GC (Agilent 7890) is equipped with a flame ion detector (FID) connected to a DB-17-ms column for the measurements of PAH species; a thermal conductivity detector (TCD) coupled to a Molsieve 5A column is used to monitor the absence of air. The GC injection system is equipped with an external valve box, which can regulate the temperature up to 320 °C, to avoid heavy species condensation during the sample storage and injection. For the second GC (Thermo Trace GC Ultra), an FID is installed and connected to an HP Plot Q column to measure small hydrocarbons, and a DSQTM (dual stage quadrupole) mass spectrometer is also connected to help the species identification.

The identification of PAH species predominantly relies on the retention time known from the prior injection of standards. The mass spectrometry provides additional information such as the mass numbers and suggests potential candidates. Figure 1 shows the GC signals in neat toluene pyrolysis, toluene-propylene and toluene-propyne co-pyrolysis at similar T_5 s around 1360 K. Not all detected signal peaks can be unambiguously identified, especially in the cases of binary fuels, where a variety of new aromatic species are introduced, in comparison to neat toluene pyrolysis. The small peaks appear before 5.5 min were also detected in toluene + acetylene/ethylene pyrolysis, and they are corresponding to vinyl-toluene ($CH_3C_6H_5C_2H_3$) and ethynyl-toluene ($CH_3C_6H_5C_2H$) isomers. A collection of C_{10} species, which mostly correspond to the small peaks between indene and naphthalene (see Fig. 1), are observed in the co-pyrolysis of toluene and propylene (or propyne). The dominant ones identified in this work

Table 1
Compositions of the experimental gas mixtures calibrated by the GC.

	Toluene (C ₇ H ₈)	Propylene (C ₃ H ₆)	Propylene (C ₃ H ₄ -P)	Impurities
Neat Toluene	105 ppm	–	–	–
Toluene+C ₃ H ₆	106 ppm	513 ppm	–	propane (C ₃ H ₈): 2 ppm
Toluene+C ₃ H ₄ -P	108 ppm	–	557 ppm	2-butene (2-C ₄ H ₈): 4.5 ppm iso-butane (i-C ₄ H ₁₀): 3.5 ppm

include methylindene isomers, dihydronaphthalene and benzofulvene. It is observed that the addition of C₃ fuels, particularly propyne, results in remarkable increases in the concentrations of indene, naphthalene and acenaphthalene. In contrast, the major PAHs in neat toluene pyrolysis appearing at this temperature (around 1360 K), such as bibenzyl and fluorene, have lower abundance. To point out, the peak at 8.45 min corresponds to biphenylmethane in neat toluene pyrolysis, but vinyl-naphthalene in toluene-C₃ co-pyrolysis.

Calibration experiments are carried out for the accurate quantification of species mole fractions. FID response for C₁–C₄ hydrocarbons (except diacetylene) and small aromatics including benzene, toluene, ethylbenzene, styrene and phenylacetylene are calibrated using purchased or homemade gas mixtures with known compositions. Diacetylene is calibrated through high-temperature pyrolysis experiments of acetylene based on carbon atoms conservation. Specific procedures, as detailed in our previous work [22], are followed to calibrate PAH species: i) calibration solutions are prepared by dissolving known amounts of specific PAHs in dichloromethane; ii) a small quantity (a few microliters) of the solution is injected into a previously vacuumed glass vessel that is heated up at 150 °C, so the solution evaporates immediately; iii) the vessel is then filled with argon to a certain pressure around 1.2 atm, and the resulting gas mixture stays for 10–15 min to homogenize; iv) the calibration gas mixture is injected to the GC at least three times to obtain consistent FID response factors for the PAHs; v) the above procedures are repeated with gas mixtures containing different PAH concentrations to derive the calibration factors. This method can be well applied to two-to-three ring PAH species, while for four-ring and larger ones, the complete vaporization cannot be guaranteed. Therefore, quantitative measurements for PAH species up to three rings, which have reliable calibration factors, are reported in the current work. The uncertainty in the quantitative measurements depend on the accuracy of the calibration. An uncertainty factor of 5%–10% is estimated for the small species directly calibrated in the gas phase, and this factor increases to 15–20% to the PAH species.

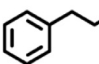
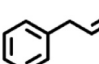
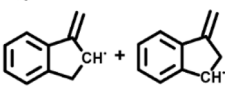
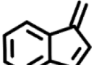
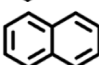
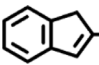
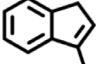
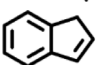
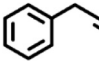
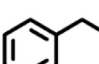
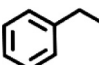
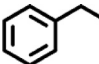
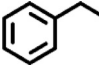
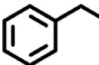
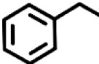
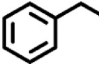
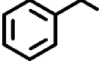
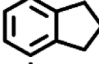
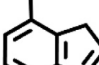
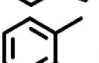
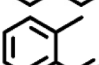
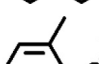


Chemicals including toluene (99.8%), propyne (97%) and PAH standards are purchased from Sigma-Aldrich. Other used gases, including propylene (99.5%), the bath gas argon (>99.9999%) and the driven gas helium (> 99.995%), are supplied by Air-Liquide. The experimental gas mixtures are prepared in a 136 L electropolished stainless steel cylinder. The cylinder is pumped to below 10^{−5} mbar using a turbo molecular pump before fuel components (toluene and C₃) are introduced. The partial pressures of the fuels are measured using a MKS Baratron pressure transducer (model 122BA) with the range of 0–10 Torr. The cylinder is subsequently filled with argon to a total pressure around 10 bar, monitored by a 0–10,000 Torr MKS Baratron pressure transducer (model 627D). The gas mixture then stays overnight before experiments to ensure good homogeneity. The exact compositions of the experimental mixtures are analyzed using the GC, and the results are listed in Table 1. The inner surface of the driven section of the shock tube is cleaned every day to remove carbon deposit. The three experimental data sets, consisting of the post-shock conditions T₅, p₅, the reaction time, the pressure time history and the species mole fractions in each shock operation, are provided in the Supplemental Material.

3. Kinetic modeling

A kinetic model has been under development in our serial works [12,22,28–30], aimed at correctly predicting the PAH formation from the pyrolysis of practical/surrogate fuels and fuel components. Updates are made in this work, mainly by extensively incorporating two groups of reactions into the kinetic model: 1. the reaction between C₃ species with C₇ radicals potentially contributing to the formation of the second aromatic ring; 2. the subsequent interactions of C₃ with the naphthyl core, which potentially further facilitate the ring growth.

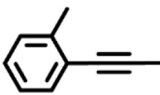
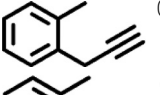
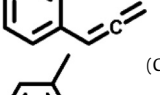
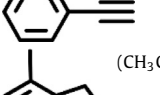
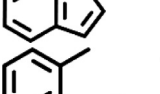
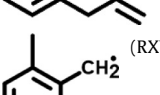
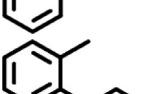
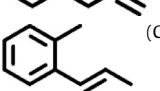
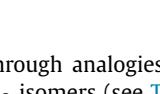
The interactions between C₃ molecule/radicals and toluene fuel radicals, namely benzyl (C₇H₇) and methylphenyl (CH₃C₆H₄), may result in a variety of products, as summarized in Table 2. Propargyl (C₃H₃) and benzyl (C₇H₇) are abundant radicals in the studied toluene-C₃ co-pyrolysis systems, due to their resonance-stabilized nature. The C₇H₇+C₃H₃ recombination reaction potential energy surface (PES) was computed at the CASPT2/cc-pVTZ//B3LYP/6–311G(d,p) level of theory in a work by Matsugi and Miyoshi [24]. A multiple-step process leading to naphthalene was proposed: the radical recombination results in two C₁₀H₁₀ monocyclic aromatic hydrocarbon (MAH) isomers, 3-butynylbenzene (C₆H₅CH₂CH₂C≡C, C₆H₅CCC#C) and 2,3-butadienylbenzene (C₆H₅CH₂CH=C=CH₂, C₆H₅CC*[•]C); 1-methylene-indanyl (C₉H₇CH₂) radicals (including two isomers, see the structures in Table 2) are formed directly through the C₇H₇+C₃H₃ reaction or via the ring closure of C₆H₅CC*[•]C; The consumption of C₉H₇CH₂ further leads to naphthalene (C₁₀H₈) and its isomer benzofulvene (C₉H₆CH₂). The mentioned reaction processes and the rate coefficients in Chebyshev form reported in [24] are used in the current kinetic model. Other C₇+C₃ reaction systems have not been studied through theoretical approaches to the best of our knowledge, so the resulting products and the corresponding rate coefficients are assessed through analogies to similar reactions. In such estimations, the similarity of C₇H₇ with allyl (C₃H₅-A) and methyl (ĊH₃) are considered. The addition of C₇H₇ to the triple bond of propyne (C₃H₄-P) resemble the C₇H₇+C₂H₂ reactions, which were theoretically studied by Mebel et al. [21]. According to the computed results in [21] and the experimental observations in our previous work [22], indene (C₉H₈) and 3-phenylpropyne (C₆H₅CH₂C≡CH) are the main products of C₇H₇ + C₂H₂ reactions. In a similar manner, for C₇H₇+C₃H₄-P reactions, a MAH species, 2-butynylbenzene (C₆H₅CH₂C≡CCH₃, C₆H₅CC*[•]CC) is formed through the side chain lengthening; and towards the formation of a cyclopenta-ring structures, besides C₉H₈+ĊH₃, 2-methylindene (C₉H₇CH₃-2)+H and 3-methylindene (C₉H₇CH₃-3)+H are also potential products, depending on which site of C₃H₄-P the C₇H₇ is added to. An alternative channel leading to the formation of 1,2-dihydronaphthalene (C₁₀H₁₀) is also considered, through an analogy to the reaction C₃H₅-A+C₃H₄-P = 1,3-cyclohexadiene(CYC₆H₈)+H. 1-phenyl-3-butene (C₆H₅CH₂CH₂CH=CH₂, C₆H₅C₄H₇-1) and 1-phenyl-2-butene (C₆H₅CH₂CH=CHCH₃, C₆H₅C₄H₇-2) are probable products from the radical recombination of C₇H₇+C₃H₅-A, and the rate coefficients are taken from the C₃H₅-A+ĊH₃ reactions forming 1-butene (1-C₄H₈) and 2-butene (2-C₄H₈), respectively. The reactions between C₇H₇ and C₃H₆ produce C₄ substituted-benzene species including the C₆H₅CH₂CH₂ĊHCH₃ (C₆H₅C₄H₈B), C₆H₅CH₂CH₂CH₂ĊH₂ (C₆H₅C₄H₈A), C₆H₅C₄H₇-1 and C₆H₅C₄H₇-2,

Table 2A list of the reactions representing the interactions between toluene fuel radicals and the C₃ radicals/molecules.

Reactants	Involved aromatic species	Reactions and the references for used rate coefficients
benzyl (C ₇ H ₇) + propargyl (C ₃ H ₃)	 (C ₆ H ₅ CCC#C)	C ₇ H ₇ +C ₃ H ₃ = C ₆ H ₅ CCC#C / C ₆ H ₅ CC [•] C [•] C / C ₉ H ₇ CH ₂ +H C ₆ H ₅ CC [•] C [•] C = C ₉ H ₇ CH ₂ +H / C ₉ H ₇ CH ₂ = C ₉ H ₆ CH ₂ +H C ₉ H ₇ CH ₂ = C ₁₀ H ₈ +H / C ₉ H ₆ CH ₂ +H = C ₁₀ H ₈ +H [24]
	 (C ₆ H ₅ CC [•] C [•] C)	
	 (C ₉ H ₇ CH ₂)	
	 (C ₉ H ₆ CH ₂)	
	 (C ₁₀ H ₈)	
benzyl (C ₇ H ₇) + propyne (C ₃ H ₄ -P)/allene (C ₃ H ₄ -A)	 (C ₉ H ₇ CH ₃ -2)	Reactions forming five-membered rings C ₇ H ₇ +C ₃ H ₄ -P = C ₉ H ₈ +CH ₃ / C ₉ H ₇ CH ₃ -2+H / C ₉ H ₇ CH ₃ -3+H: analogies to C ₇ H ₇ +C ₂ H ₂ = C ₉ H ₈ +H [21]. Reactions lengthening of the side chain C ₇ H ₇ +C ₃ H ₄ -P = C ₆ H ₅ CC#CC+H, C ₇ H ₇ +C ₃ H ₄ -A = C ₆ H ₅ CC [•] C [•] C+H: analogies to C ₇ H ₇ +C ₂ H ₂ = C ₆ H ₅ C ₃ H ₃ P_3 +H [21].
	 (C ₉ H ₇ CH ₃ -3)	
	 (C ₉ H ₈)	
	 (C ₆ H ₅ CC#CC)	
	 (C ₆ H ₅ CC [•] C [•] C)	
benzyl (C ₇ H ₇) + allyl (C ₃ H ₅ -A)	 (C ₆ H ₅ C ₄ H ₇ -1)	C ₇ H ₇ +C ₃ H ₅ -A(+M) = C ₆ H ₅ C ₄ H ₇ -1(+M): analogies to CH ₃ +C ₃ H ₅ -A = C ₄ H ₈ -1 from the core mechanism [35] C ₆ H ₅ C ₄ H ₇ -2 = C ₇ H ₇ +C ₃ H ₅ -A / C ₄ H ₈ -2 = CH ₃ +C ₃ H ₅ -A from the core mechanism [35]
	 (C ₆ H ₅ C ₄ H ₇ -2)	
	 (C ₆ H ₅ C ₄ H ₇ -1)	
benzyl (C ₇ H ₇) + propene (C ₃ H ₆)	 (C ₆ H ₅ C ₄ H ₈ A)	C ₇ H ₇ +C ₃ H ₆ = C ₆ H ₅ C ₄ H ₈ A / C ₆ H ₅ C ₄ H ₈ B / C ₆ H ₅ C ₄ H ₇ -1+H / C ₆ H ₅ C ₄ H ₇ -2+H / C ₆ H ₅ C ₂ H ₄ +C ₂ H ₄ : analogies to CH ₃ +C ₃ H ₆ = PC ₄ H ₉ / SC ₄ H ₉ / C ₄ H ₈ -1+H / C ₄ H ₈ -2+H / C ₂ H ₅ +C ₂ H ₄ from the core mechanism [35] C ₇ H ₇ +C ₃ H ₆ = C ₉ H ₁₀ +H: analogy to C ₃ H ₅ -A+C ₃ H ₆ (+M) = CYC ₅ H ₈ +CH ₃ (+M) [32]
	 (C ₆ H ₅ C ₄ H ₈ B)	
	 (C ₆ H ₅ C ₄ H ₇ -1)	
	 (C ₆ H ₅ C ₄ H ₇ -2)	
	 (C ₆ H ₅ C ₂ H ₄)	
	 (C ₉ H ₁₀)	
	 (CH ₃ C ₉ H ₇)	
methyl phenyl (CH ₃ C ₆ H ₄) + propargyl (C ₃ H ₃)	 (CH ₃ C ₆ H ₄ C ₃ H ₃ P_3)	CH ₃ C ₆ H ₄ +C ₃ H ₃ = CH ₃ C ₉ H ₇ / CH ₃ C ₆ H ₄ C ₃ H ₃ P_3 / CH ₃ C ₆ H ₄ C ₃ H ₃ A+H / CH ₃ C ₆ H ₄ C ₃ H ₂ +H: analogies to C ₆ H ₅ +C ₃ H ₃ = C ₉ H ₈ / C ₆ H ₅ C ₃ H ₃ P_3 / C ₆ H ₅ C ₃ H ₃ A / C ₆ H ₅ C ₃ H ₂ [33]
	 (CH ₃ C ₆ H ₄ C ₃ H ₃ A)	
	 (CH ₃ C ₆ H ₄ C ₃ H ₂)	
	 (CH ₃ C ₆ H ₄ C ₃ H ₂)	

(continued on next page)

Table 2 (continued)

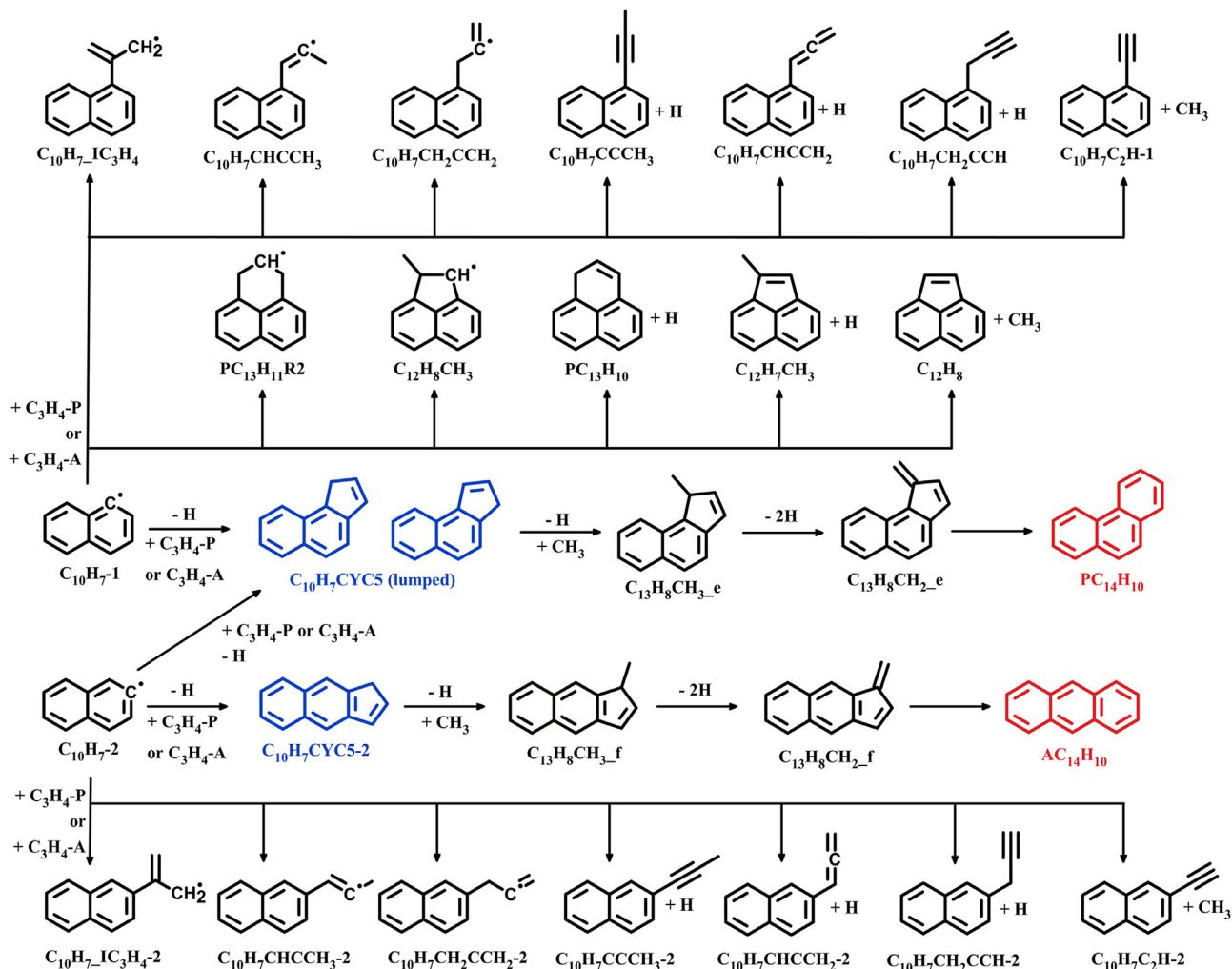
Reactants	Involved aromatic species	Reactions and the references for used rate coefficients
methyl phenyl ($\text{CH}_3\text{C}_6\text{H}_4$) + propyne ($\text{C}_3\text{H}_4\text{-P}$)/allene ($\text{C}_3\text{H}_4\text{-A}$)	 ($\text{CH}_3\text{C}_6\text{H}_4\text{C}_3\text{H}_3\text{P}_1$)	$\text{CH}_3\text{C}_6\text{H}_4 + \text{C}_3\text{H}_4\text{-P} = \text{CH}_3\text{C}_6\text{H}_4\text{C}_3\text{H}_3\text{P}_1 + \text{H}$ / $\text{CH}_3\text{C}_6\text{H}_4\text{C}_3\text{H}_3\text{A} + \text{H}$ / $\text{CH}_3\text{C}_6\text{H}_4\text{C}_2\text{H} + \dot{\text{C}}\text{H}_3$ / $\text{CH}_3\text{C}_9\text{H}_7 + \text{H}$: analogies to $\text{C}_6\text{H}_5 + \text{C}_3\text{H}_4\text{-P} = \text{C}_6\text{H}_5\text{C}_3\text{H}_3\text{P}_1 + \text{H}$ / $\text{C}_6\text{H}_5\text{C}_3\text{H}_3\text{A} + \text{H}$ / $\text{C}_6\text{H}_5\text{C}_2\text{H} + \dot{\text{C}}\text{H}_3$ / $\text{C}_9\text{H}_8 + \text{H}$ [21] $\text{CH}_3\text{C}_6\text{H}_4 + \text{C}_3\text{H}_4\text{-A} = \text{CH}_3\text{C}_6\text{H}_4\text{C}_3\text{H}_3\text{P}_3 + \text{H}$ $\text{CH}_3\text{C}_6\text{H}_4\text{C}_2\text{H} + \dot{\text{C}}\text{H}_3$ / $\text{CH}_3\text{C}_6\text{H}_4\text{C}_3\text{H}_3\text{A} + \text{H}$ / $\text{CH}_3\text{C}_9\text{H}_7 + \text{H}$: analogies to $\text{C}_6\text{H}_5 + \text{C}_3\text{H}_4\text{-A} = \text{C}_6\text{H}_5\text{C}_3\text{H}_3\text{P}_3 + \text{H}$ $\text{C}_6\text{H}_5\text{C}_2\text{H} + \dot{\text{C}}\text{H}_3$ / $\text{C}_6\text{H}_5\text{C}_3\text{H}_3\text{A} + \text{H}$ / $\text{C}_9\text{H}_8 + \text{H}$ [21]
	 ($\text{CH}_3\text{C}_6\text{H}_4\text{C}_3\text{H}_3\text{P}_3$)	
	 ($\text{CH}_3\text{C}_6\text{H}_4\text{C}_3\text{H}_3\text{A}$)	
	 ($\text{CH}_3\text{C}_6\text{H}_4\text{C}_2\text{H}$)	
	 ($\text{CH}_3\text{C}_9\text{H}_7$)	
methyl phenyl ($\text{CH}_3\text{C}_6\text{H}_4$) + allyl ($\text{C}_3\text{H}_5\text{-A}$)	 ($\text{CH}_3\text{C}_6\text{H}_4\text{C}_3\text{H}_5\text{-1}$)	$\text{CH}_3\text{C}_6\text{H}_4 + \text{C}_3\text{H}_5\text{-A} = \text{CH}_3\text{C}_6\text{H}_4\text{C}_3\text{H}_5\text{-1}$ / $\text{RXYLENE} + \text{C}_2\text{H}_3$: analogies to $\text{C}_6\text{H}_5 + \text{C}_3\text{H}_5\text{-A} = \text{C}_6\text{H}_5\text{C}_3\text{H}_5\text{-1}$ / $\text{C}_7\text{H}_7 + \text{C}_2\text{H}_3$ [34]
	 (RXYLENE)	
methyl phenyl ($\text{CH}_3\text{C}_6\text{H}_4$) + propene (C_3H_6)	 ($\text{CH}_3\text{C}_6\text{H}_4\text{C}_3\text{H}_5\text{-1}$)	$\text{CH}_3\text{C}_6\text{H}_4 + \text{C}_3\text{H}_6 = \text{CH}_3\text{C}_6\text{H}_4\text{C}_3\text{H}_5\text{-1} + \text{H}$ / $\text{CH}_3\text{C}_6\text{H}_4\text{C}_3\text{H}_5\text{-2} + \text{H}$: analogies to $\text{C}_6\text{H}_5 + \text{C}_3\text{H}_6 = \text{C}_6\text{H}_5\text{C}_3\text{H}_5\text{-1} + \text{H}$ / $\text{C}_6\text{H}_5\text{C}_3\text{H}_5\text{-2} + \text{H}$ [21]
	 ($\text{CH}_3\text{C}_6\text{H}_4\text{C}_3\text{H}_5\text{-2}$)	

and the rate coefficients are determined through analogies to the $\text{CH}_3 + \text{C}_3\text{H}_6$ reactions forming C_4H_9 and C_4H_8 isomers (see Table 2). Another reaction, $\text{C}_7\text{H}_7 + \text{C}_3\text{H}_6 = \text{indane (C}_9\text{H}_{10}) + \text{H}$, is also taken into account, which is analogous the five membered ring formation process of $\text{C}_3\text{H}_5\text{-A} + \text{C}_3\text{H}_6 = \text{cyclopentene (CYC}_5\text{H}_8) + \text{H}$ [32]. Reactions between C_3 species and methylphenyl involve the radical site on the benzene ring, and thus the reactions and corresponding rate coefficients are assessed through analogies to the reactions between phenyl (C_6H_5) and C_3H_{3-6} species based on the serial theoretical works by Mebel and coworkers [21,33,34]. Only *o*-methylphenyl related reactions are considered and shown in Table 2 for simplification purpose.

As mentioned in the experimental section, naphthalene (C_{10}H_8) is measured of significant concentrations in toluene-propyne copolyrolysis. In the current kinetic model, two types of naphthyl radicals, 1-naphthyl ($\text{C}_{10}\text{H}_7\text{-1}$) and 2-naphthyl ($\text{C}_{10}\text{H}_7\text{-2}$), which lead to different reaction pathways and consequent species, are separately considered. Rate coefficients for hydrogen abstraction reactions by H atom from C_{10}H_8 forming the two radicals are from [36], and those for the decomposition and isomerization of the C_{10}H_7 radicals are from [37]. The interactions between naphthyl radicals and propyne/allene/propargyl are also considered. Raj et al. [38] mapped out a step-wise formation scheme of the $\text{C}_{13}\text{H}_{10}$ isomers, phenalene ($\text{PC}_{13}\text{H}_{10}$) and 1-methylene-1,2-dihydroacenaphthalene ($\text{C}_{12}\text{H}_8\text{CH}_2$), which is initiated by C_3H_3 addition to naphthalene and naphthyl radical. Both $\text{C}_{13}\text{H}_{10}$ species and relevant intermediates are also involved in the reaction system of $\text{CH}_3 + 1\text{-acenaphthyl (C}_{12}\text{H}_7)$, which was studied in a recent theoretical work by Porfiriev et al. [39]. All above-mentioned reactions and the corresponding rate coefficients are integrated in the current model. The current kinetic model also incorporates reactions between naphthyl radicals ($\text{C}_{10}\text{H}_7\text{-1}$ and $\text{C}_{10}\text{H}_7\text{-2}$) react

with propyne/allene, as shown in Scheme 1. The reactions between $\text{C}_{10}\text{H}_7\text{-1}$ and $\text{C}_3\text{H}_4\text{-P/C}_3\text{H}_4\text{-A}$ are studied in a recent work by Zhao et al. [40], and the reported theoretical rate coefficients are used in the current model. The relevant reactions involve the formation of a side chain or a fused ring on the naphthyl core, yielding a variety of products such as C_3 substituted naphthyl species, cyclopentane-fused structures and phenalene ($\text{PC}_{13}\text{H}_{10}$). Similar reaction pathways are expected in the $\text{C}_{10}\text{H}_7\text{-2} + \text{C}_3\text{H}_4\text{-P/C}_3\text{H}_4\text{-A}$ system, except that $\text{PC}_{13}\text{H}_{10}$ cannot be formed (see Scheme 1). The ring expansion by methylation can occur to the cyclopentane-fused species, $\text{C}_{10}\text{H}_7\text{-CYC}_5$ and $\text{C}_{10}\text{H}_7\text{-CYC}_5\text{-2}$, eventually forming phenanthrene ($\text{PC}_{14}\text{H}_{10}$) and anthracene ($\text{AC}_{14}\text{H}_{10}$), respectively. Such processes are estimated through analogies to the reactions of indenyl (C_9H_7)+methyl (CH_3) leading to naphthalene [21,41].

For the newly introduced species, thermochemical properties are computed using the program "THERM" [42] with the group values updated by Burke et al. [43] recently. The reaction mechanism and the species thermochemical data of the current kinetic model are provided in the Supplemental Material. Simulations presented in the discussion section are conducted with the homogenous reactor model of the software COSILAB [44] using a constant pressure of 20 bar and a nominal reaction time of 4.0 ms. Such a simplification has been well justified in relevant publications [45,46], and well applies to the current experimental configurations. Figure S2 shows the time-dependent fuel (C_3 fuels and toluene) mole fractions under specific experimental conditions simulated via two methods: the above-mentioned simplified practice and using the measured pressure profiles up to 10 ms together with the measured T_5 at zero point. It is seen that the end-point mole fractions at 4 ms agree well with the plateau values of the extended simulations, and actually the variations are smaller than the experimental errors. A concern may still



Scheme 1. Reactions between naphthyl radicals and propyne/allene that are considered in the kinetic model.

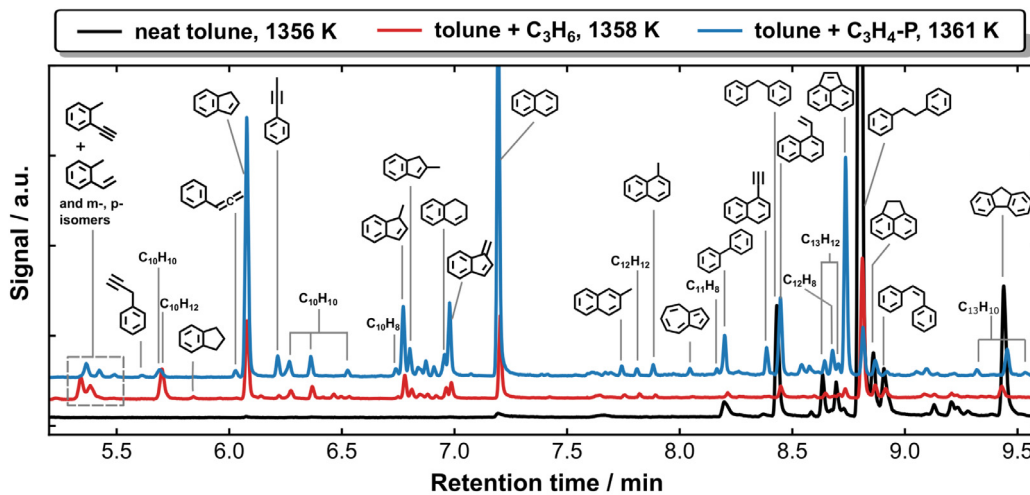


Fig. 1. GC signals recorded in neat toluene, toluene + propylene (C_3H_6) and toluene + propyne (C_3H_4-P) pyrolysis at T_5 around 1360 K.

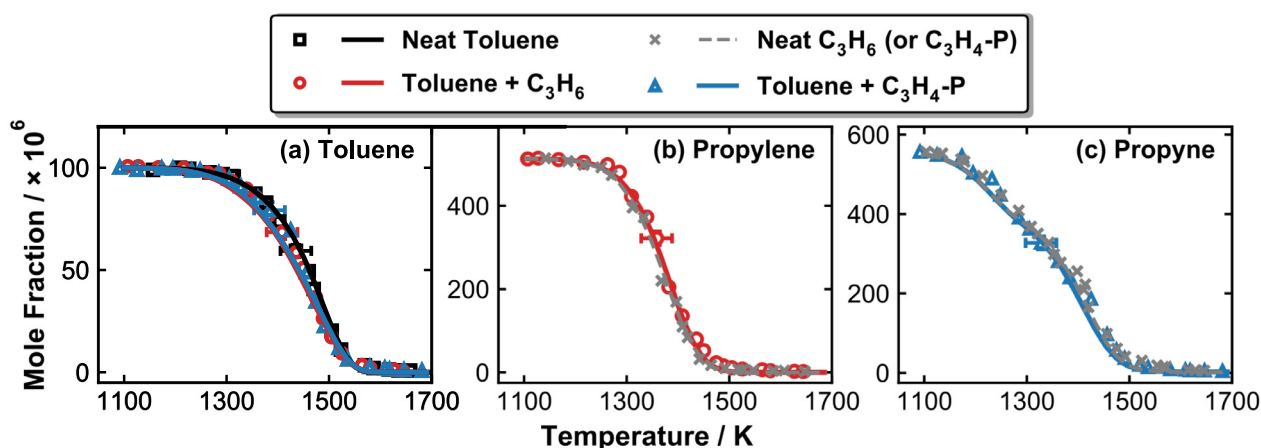


Fig. 2. Measured (symbols) and simulated (solid lines) mole fractions for fuels in three experimental sets. Initial toluene mole fractions are all normalized to 100 ppm to facilitate comparison in (a) and mole fraction profiles of propylene and propyne in the pyrolysis of neat C_3 fuels [28] are given in (b) and (c).

arise that specific radical-radical recombination reactions would continue after the arrival of rarefaction waves and impact the final observed species mole fractions [22,28,30]. Therefore, simulations are performed using pressure profiles up to 10 ms, mainly to monitor the influences of the reactions during the post-shock quenching. Such effects are significant for a few species whose formation depends on the recombination of resonance-stabilized radicals or methyl, such as bibenzyl and 1-methylindene. Relevant results will be displayed and discussed in the following section.

4. Results and discussion

In this section, the predictive performances of the kinetic model will be tested using the current speciation measurements. The measured species pools in the three studied cases, which consist of different types and quantities of pyrolysis products, will be compared. Modeling analyses will help to identify the specific reactions that are responsible for the observed differences. Discussion will be focused on the interactions between C_3 species and toluene as well as relevant radicals, which potentially impact the fuel decomposition reactivity and speciation behaviors. To point out, since the three studied reaction systems contain different amounts of carbon atoms, direct comparisons of the absolute species mole fractions require more caution.

4.1. Fuel decomposition reactivity

Figure 2 illustrates the experimental and simulated fuel mole fractions as a function of the post-shock temperature T_5 in all three studied cases. The initial toluene mole fractions in the three different experimental sets are normalized to 100 ppm to facilitate comparisons. Besides, the conversion profiles of C_3 fuels in neat propylene and neat propyne pyrolysis reported in our recent work [28] are also given as a reference. The current kinetic model can satisfactorily capture the temperature-dependent mole fraction measurements of individual fuels in all studied cases. Given an uncertainty of ± 30 K in T_5 s, different toluene decomposition reactivity among the three cases cannot be definitively judged from the largely overlapping experimental profiles. The kinetic model, however, predicts higher conversion rates of toluene in the cases of binary fuel pyrolysis over the temperature range of 1300–1500 K. In contrast, the presence of toluene barely changes the conversion rates of propylene and propyne. As discussed in our previous work [28], the decomposition of propylene follows a regular smooth curve, while the decay of propyne exhibits a unique

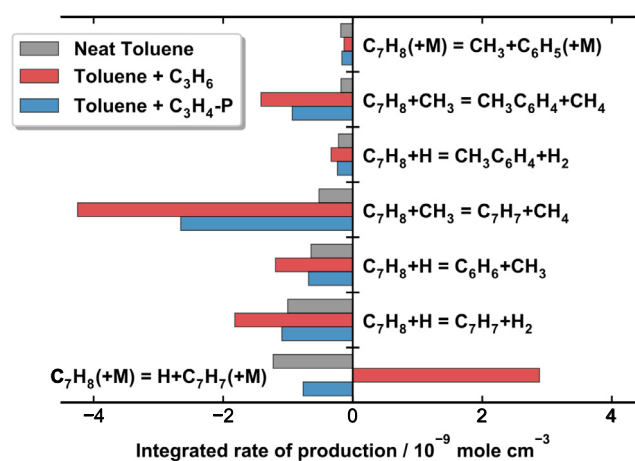


Fig. 3. Integrated rate of production coefficients for toluene in neat toluene pyrolysis, toluene-propylene co-pyrolysis and toluene-propyne co-pyrolysis at T_5 of 1400 K.

two-stage nature due to the isomerization to allene at relatively low temperatures. As will be shown later, at the temperatures corresponding to the first stage of propyne decomposition, propyne mostly converts to allene so that radicals are only formed in a limited amount.

Rate-of-production (ROP) analyses are performed to investigate the reasons for the changed toluene decomposition reactivity, and the major toluene consumption pathways at T_5 of 1400 K in the three cases are shown in Fig. 3. In neat toluene pyrolysis at 1400 K, the C–H bond fission and the hydrogen abstraction by H, which both produce benzyl (C_7H_7), dominate the consumption of toluene. In toluene-propylene (or propyne) co-pyrolysis at the same temperature, the importance of hydrogen abstraction reactions is substantially enhanced. In particular, the hydrogen abstraction by $\dot{C}H_3$ forming C_7H_7 is found as the predominant toluene decomposition channel. The reason lies in the fact that the pyrolysis of propylene (or propyne) significantly increase the level of H and $\dot{C}H_3$. A large amount of $\dot{C}H_3$ is formed through the addition-elimination reaction $C_3H_x + H = C_2H_{x-2} + \dot{C}H_3$ ($x = 4, 6$), which is an essential fuel consumption pathway in propylene and propyne pyrolysis [28]. It is remarkable that the reaction $C_7H_8(+M) = H + C_7H_7(+M)$ becomes a C_7H_8 formation pathway in toluene-propylene co-pyrolysis. This is because C_7H_7 radicals

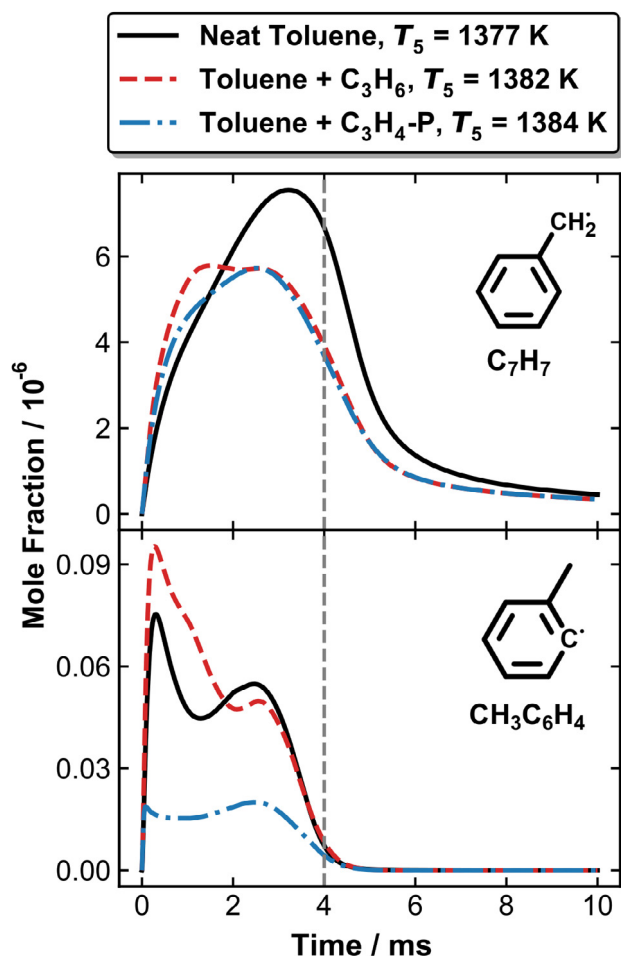


Fig. 4. Simulated time-dependent mole fractions of toluene fuel radicals using measured pressure profiles in neat toluene pyrolysis and toluene-C₃ fuel co-pyrolysis. The vertical dashed lines indicate the nominal reaction time of 4.0 ms.

produced through hydrogen abstraction reactions recombine with H atoms that are abundant in this reaction system. Compared to the case of neat toluene pyrolysis, the production of the other type of toluene fuel radical, methyl-phenyl (CH₃C₆H₄), also increases through the intensified hydrogen abstraction channels in toluene-C₃ co-pyrolysis. As for the C₃ fuels, the ROP-analyzed consumption schemes are very similar to those in neat propylene and propyne pyrolysis [28]. Toluene chemistry has negligible impacts on propylene decomposition, and the reactions with benzyl contribute to less than 3% of propyne consumption at T₅ of 1400 K.

Figure 4 presents the simulated time-dependent mole fractions of C₇H₇ and CH₃C₆H₄ using measured pressure profiles up to 10 ms at T₅s around 1380 K in all three studied cases. It is seen that C₇H₇ is much more abundant than CH₃C₆H₄, and it remains in relatively high concentrations by the end of the defined reaction time, and the consumption of C₇H₇ extends into the quenching period. In a different manner, the consumption of CH₃C₆H₄ almost completes by the end of the reaction time of 4 ms. In all shown cases, the time-dependent CH₃C₆H₄ concentration profiles exhibit double peak behaviors. ROP analyses at the time points corresponding to both peaks show that the formation of CH₃C₆H₄ rely on hydrogen abstractions from toluene by H and CH₃, while the isomerization to C₇H₇ is a consumption channel. The second peak of CH₃C₆H₄ concentrations is attributed to the changed pressure/temperature during the reaction time: the measured pressure

profile always shows a small rise before the arrival of the quenching wave in our experiments. This results in an enhanced consumption rate of toluene and thus a second increase in CH₃C₆H₄ concentrations. With relatively small concentrations, the reactions of CH₃C₆H₄ may not significantly impact the composition of the final species pools. Compared to the case of neat toluene pyrolysis, C₇H₇ is formed more rapidly at the initial stage of the reaction duration in toluene-C₃ co-pyrolysis, although it reaches lower peak mole fractions. This suggests that a large portion of C₇H₇ reacts away with the species introduced by the addition of propylene (or propyne), despite an enhanced formation via hydrogen abstraction reactions from toluene.

ROP analyses are performed for both C₇H₇ and CH₃C₆H₄ in each studied case with two different methods: I. using constant T₅ of 1380 K and p₅ of 20 bar over a nominal reaction time of 4 ms; II. employing the measured pressure profiles up to 10 ms with the zero point temperatures set at the measured T₅s around 1380 K (1377 K, 1382 K and 1384 K in neat toluene, toluene + C₃H₆ and toluene + C₃H₄-P pyrolysis, respectively). The ROP coefficients are then integrated over the reaction time, yielding the species production (consumption) amounts. The results for C₇H₇ is shown in Fig. 5 and those for CH₃C₆H₄ are provided in Fig. S3 in the Supplementary Material. Different information can be probed from the analyzed results, such as the reactions occurring in the post-shock quenching and the influences brought by different fuel compositions. It is seen that the C₇H₇ self-recombination leading to bibenzyl (C₆H₅C₂H₄C₆H₅) mostly proceeds during the quenching periods. This reaction is found as the predominant C₇H₇ sink in neat toluene pyrolysis when the post-shock quenching is considered in the analysis. The dissociation into C₇H₆+H is the main C₇H₇ consumption channel over the defined reaction time of 4 ms, which however does not continue after the arrival of the rarefaction waves. In toluene-C₃ co-pyrolysis, the major C₇H₇ consumption pathways shift to other reactions. The relative importance of C₇H₇+CH₃ recombination increases remarkably, because of the sufficient CH₃ production from propylene (or propyne) decomposition, as discussed above. In toluene-propylene co-pyrolysis, the C₇H₇+H recombination dominates the consumption of C₇H₇ due to the high concentrations of H atoms, regardless of the analyzing methods. The newly introduced reactions between C₇H₇ and C₃H₄-P play an important role in C₇H₇ consumption in toluene-propyne co-pyrolysis. Overall, the addition of propylene (or propyne) facilitates C₇H₇ consumption by enhancing radical levels or bringing about new reaction channels. This also accounts for the lower C₇H₇ concentrations (after 2 ms) in toluene-C₃ co-pyrolysis (see Fig. 4(a)).

As for the consumption of CH₃C₆H₄, the relative importance of different reactions is not obviously changed when different analyzing methods are used. In neat toluene pyrolysis, CH₃C₆H₄ is mainly consumed through the recombination with C₇H₇, while the reactions with allyl (C₃H₅-A) and C₃H₄-P become the most important sinks for CH₃C₆H₄ in toluene-propylene and toluene-propyne co-pyrolysis, respectively. It is seen that the addition of propylene slightly increases the mole fractions of CH₃C₆H₄ in comparison to neat toluene pyrolysis, whereas the addition of propyne has the opposite effects. Much more CH₃C₆H₄ radicals are produced through hydrogen abstraction reactions with the addition of C₃ fuels, in particular propylene. Nevertheless, in toluene-propyne co-pyrolysis, the increased CH₃C₆H₄ production cannot compensate for the remarkable consumption via the reactions with C₃H₄-P.

4.2. Small species and mono-aromatic hydrocarbons (MAHs)

Experimental and simulated mole fractions for small molecule intermediates, including C₁-C₆ non-aromatic hydrocarbons, are given in Fig. 6. Only a few small species are observed in neat

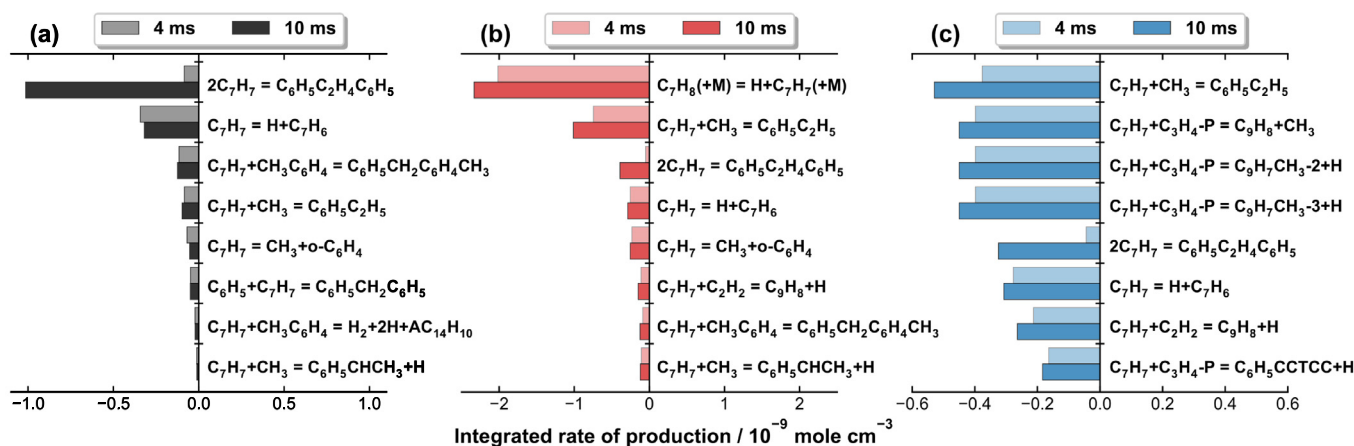


Fig. 5. Integrated ROP coefficients of benzyl (C_7H_7) over a reaction time of 4 ms at a constant p_5 of 20 bar and T_5 of 1380 K, and over 10 ms by using measured pressure profiles at T_5 s around 1380 K in (a) neat toluene pyrolysis, (b) toluene-propylene co-pyrolysis and (c) toluene-propyne co-pyrolysis.

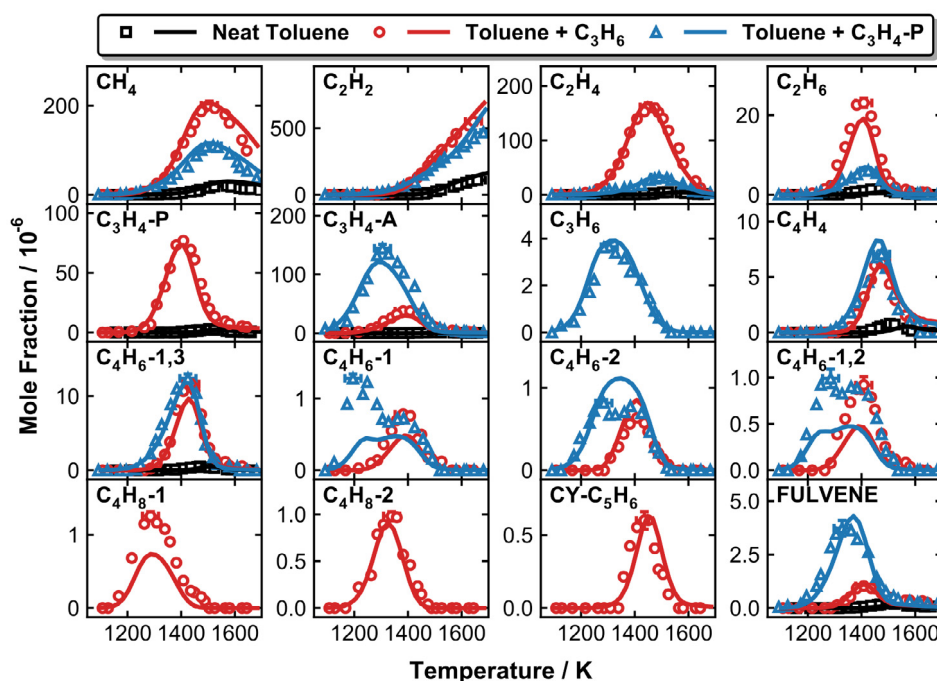


Fig. 6. Measured (symbols) and simulated (solid lines) mole fractions for small species in neat toluene, toluene + C_3H_6 and toluene + C_3H_4-P pyrolysis.

toluene pyrolysis, while the addition of propylene (or propyne) increases the diversity and abundance of small hydrocarbon intermediates. The kinetic model can well predict the absolute mole fractions as well as the relevant amounts among the three experimental sets. The types of small intermediates in toluene-propylene and toluene-propyne co-pyrolysis are the same with those in neat propylene and neat propyne pyrolysis [28], respectively. The remarkable mole fractions of methane (CH_4) and ethane (C_2H_6) measured in toluene-propylene co-pyrolysis experiments arise from the plentiful $\dot{C}H_3$ production via $H+C_3H_6 = \dot{C}H_3+C_2H_4$, which also account for the abundance of ethylene (C_2H_4). Since propyne (C_3H_4-P) is among the decomposition products of propylene, all small species detected in toluene-propyne co-pyrolysis are also seen in toluene-propylene co-pyrolysis. Butene isomers, 1-butene (C_4H_8-1) and 2-butene (C_4H_8-2), and cyclopentadiene (CYC_5H_6) are only observed in toluene-propylene pyrolysis, because their formation relies on the reactions of propylene (C_3H_6) and allyl (C_3H_5-A). C_4H_8-

1 is formed mainly via the $C_3H_5-A+\dot{C}H_3$ recombination and the reverse reaction of $C_4H_8-1+H = C_3H_6+\dot{C}H_3$, and the latter channel ($C_3H_6+\dot{C}H_3$) also leads to the formation of C_4H_8-2 . CYC_5H_6 is produced mainly through the dehydrogenation of cyclopentene (CYC_5H_8), which comes from the isomerization of 3-pentadiene (LC_5H_8) following the reverse reaction of $LC_5H_8+H = C_3H_6+C_2H_3$. Fulvene has negligible amounts in neat toluene pyrolysis, while the addition of propylene (or propyne) significantly enhances fulvene mole fractions through propargyl (C_3H_3) self-recombination and $C_3H_3+C_3H_5-A$ recombination.

Quantitative measurements for mono-ring aromatic hydrocarbon (MAH) products and the corresponding simulations are presented in Fig. 7. Similar to the case of the small hydrocarbons, the presence of propylene (or propyne) also increases the amounts of MAHs that are already observed in neat toluene pyrolysis and introduces new types of MAHs. The kinetic model exhibits a satisfactory performance in reproducing the measured MAHs mole

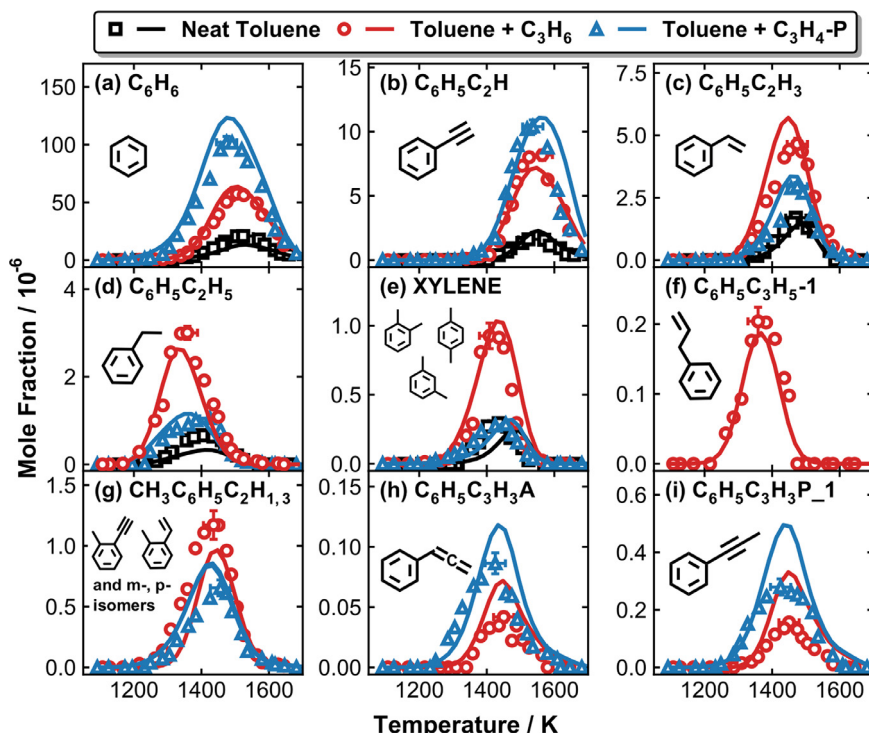


Fig. 7. Measured (symbols) and simulated (solid lines) mole fractions for MAHs in neat toluene, toluene + C_3H_6 and toluene + C_3H_4 -P pyrolysis.

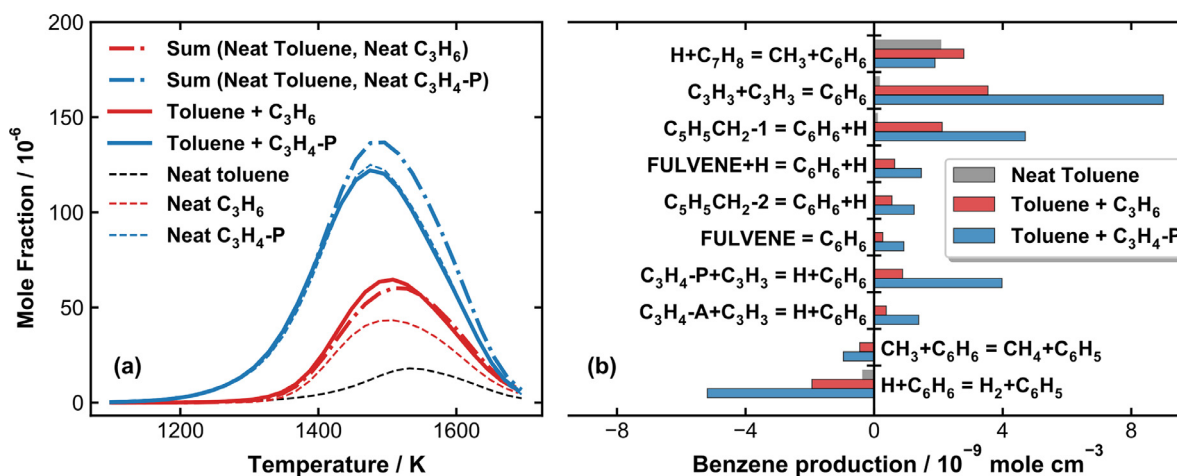


Fig. 8. (a) Simulated benzene mole fractions in the pyrolysis of neat fuel components (thin dashed lines): toluene (105 ppm in argon), propylene (513 ppm in argon), propyne (557 ppm in argon). The summed benzene mole fraction in neat toluene and neat C_3 fuel (dash dotted lines) are compared with the simulated benzene mole fractions in toluene- C_3 co-pyrolysis (solid lines). (b) Integrated ROP analyses for benzene in neat toluene pyrolysis, toluene-propylene and toluene-propyne co-pyrolysis at T_5 of 1500 K.

fraction profiles. Benzene (C_6H_6) is among the major products in individual cases, and the added C_3 fuels have two-fold effects on C_6H_6 speciation: enhancing the peak mole fractions and lowering the temperature window. In Fig. 8(a), simulated C_6H_6 mole fractions in neat toluene pyrolysis and neat C_3 fuel (either propylene or propyne) pyrolysis are summed up and compared with those in toluene-propylene (or propyne) co-pyrolysis. The C_6H_6 mole fractions in toluene-propylene co-pyrolysis are slightly higher than the summed C_6H_6 mole fractions in the pyrolysis of neat fuel components, while the opposite is seen in the case of toluene + propyne. This suggests that there are interactions between toluene and propylene (or propyne), which influence the final C_6H_6 mole fractions. The rate-of-production analyses of benzene at T_5 of 1500 K in the three studied cases are shown in Fig. 8(b). In neat toluene pyrolysis, C_6H_6 is almost exclusively produced through the ipso-

substitution reaction $H+C_7H_8 = CH_3+C_6H_6$, while in toluene-propylene (propyne) co-pyrolysis, C_3H_3 self-recombination reaction becomes the dominant channel. In toluene-propylene co-pyrolysis, the C_6H_6 formation through the $H+C_7H_8$ channel also increases, compared to that in neat toluene pyrolysis, which is attributed to the much higher production of H atoms. This may account for the synergistic effects of toluene and propylene in facilitating C_6H_6 formation. In toluene-propyne co-pyrolysis, C_6H_6 formation largely relies on C_3+C_3 reactions, while the presence of toluene results in a portion of C_3H_4 -P reacting with C_7H_7 , as discussed above. Therefore, compared to neat propyne pyrolysis, the contribution of C_3H_4 -P reactions to C_6H_6 formation is reduced. Eventually, less C_6H_6 is produced in toluene-propyne co-pyrolysis than the summed C_6H_6 production in neat toluene and neat propyne pyrolysis (see Fig. 8(a)).

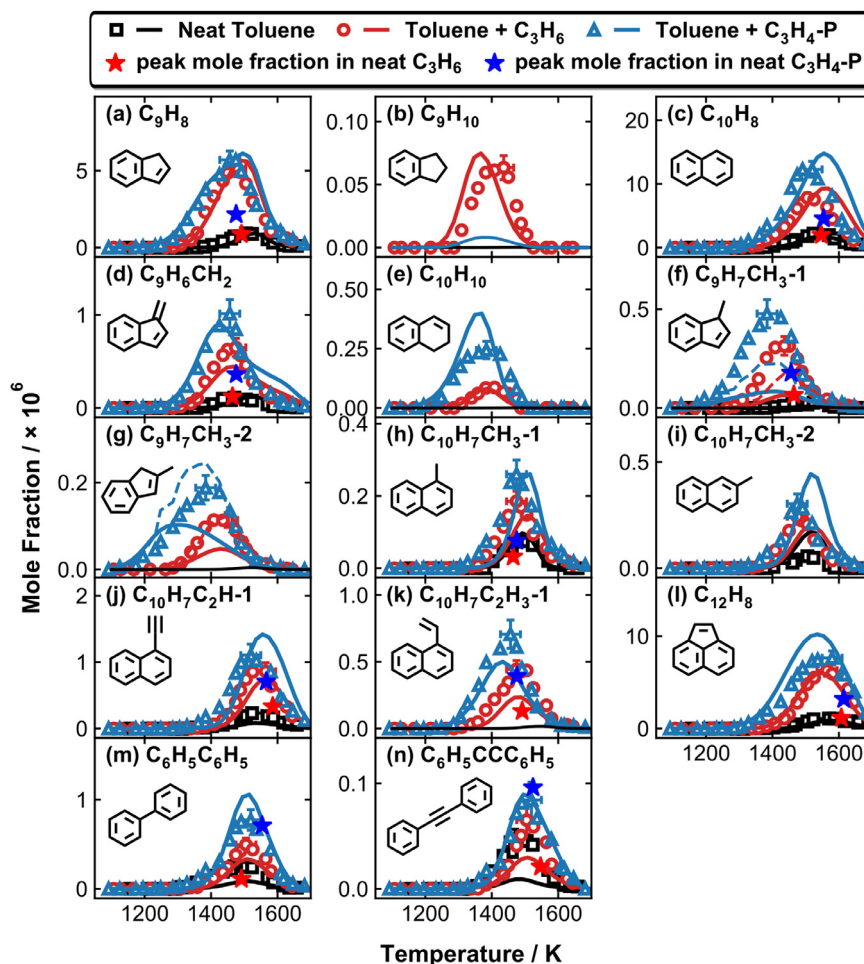


Fig. 9. Measured (symbols) and simulated (solid lines) mole fractions of the first group of PAH species in neat toluene, toluene + C_3H_6 and toluene + C_3H_4 -P pyrolysis. For $C_9H_7CH_3$ -1 and $C_9H_7CH_3$ -2, whose mole fractions are significantly influenced by the reactions during the quenching period, simulated mole fractions using the measured pressure profiles up to 10 ms (dashed lines) are also presented. Measured PAH peak mole fractions in neat propylene and propyne pyrolysis come from [28], with initial C_3 fuel concentrations being normalized to the same with those in toluene-propylene (or propyne) pyrolysis.

Ethylbenzene ($C_6H_5C_2H_5$) and xylene isomers (XYLENE) are formed via $C_7H_7 + CH_3$ and $CH_3C_6H_4 + CH_3$ recombination reactions, respectively. In toluene-propylene co-pyrolysis, the formation of both types of toluene fuel radicals, C_7H_7 and $CH_3C_6H_4$, is enhanced thanks to the intensified hydrogen abstraction reactions. Besides, the dominant propylene consumption channel through $H + C_3H_6 = CH_3 + C_2H_4$ results in a considerable amount of CH_3 . Hence, the mole fractions of the C_8H_{10} isomers ($C_6H_5C_2H_5$ and XYLENE) are much higher than those in neat toluene and toluene + propyne pyrolysis. The production of both styrene ($C_6H_5C_2H_3$) and phenylacetylene ($C_6H_5C_2H$) is enhanced by the added C_3 fuels, in comparison to that in neat toluene pyrolysis. More specifically, the highest $C_6H_5C_2H_3$ and $C_6H_5C_2H$ mole fractions are observed in toluene-propylene and toluene-propyne co-pyrolysis, respectively. The formation of $C_6H_5C_2H_3$ and $C_6H_5C_2H$ largely depends on the $C_6H_5 + C_2H_x$ ($x = 4, 2$) reactions, and the pyrolysis of propylene (or propyne) enhances the concentrations of the precursors, C_6H_5 and C_2H_x , in the reaction system, and therefore facilitates the production of $C_6H_5C_2H_3$ and $C_6H_5C_2H$. Besides, the decomposition of $C_6H_5C_2H_5$ is also an important source of $C_6H_5C_2H_3$ in toluene-propylene co-pyrolysis, because of the increased $C_6H_5C_2H_5$ production. Larger (more than C_9) MAHs are not observed in neat toluene pyrolysis, but are identified in the pyrolysis of toluene- C_3 binary mixtures. Allylbenzene ($C_6H_5C_3H_5$ -1), which comes from the $C_6H_5 + C_3H_6$ and $C_6H_5 + C_3H_5$ -A reactions, is only seen in toluene-propylene pyrolysis. A bunch of

small peaks with the formulas of C_9H_8 and C_9H_{10} with retention time of 5.3–5.4 min (see Fig. 1) are observed in both toluene+ C_3 and toluene+ C_2 [22] pyrolysis experiments. Mass spectra suggest that they have ethynyl- or vinyl- toluene structures, though the o-, m- or p- type isomers cannot be unambiguously specified. Besides, some of these C_9H_8 and C_9H_{10} species have close retention time so the signals are overlapped. Therefore, the total mole fraction measurements of all these small peaks are given in Fig. 7(g). The simulated ethynyl toluene ($CH_3C_6H_4C_2H$) and vinyl toluene ($CH_3C_6H_4C_2H_3$) are summed up to compare with the experimental profile, and a good agreement is seen between the measured and modeling results. The detection of such species indicates the interactions between $CH_3C_6H_4$ and C_2 species. Other C_9H_8 isomers, 1-phenylpropyne ($C_6H_5C_3H_3$ -P_1) and phenylallene ($C_6H_5C_3H_3$ -A), are detected in both toluene-propylene and toluene-propyne co-pyrolysis. Both species start to form at lower temperatures and have higher peak mole fractions in toluene-propyne pyrolysis, since they mainly result from the $C_6H_5 + C_3H_4$ -P reactions.

4.3. Polycyclic aromatic hydrocarbon (PAH) species

All PAH species observed in the current experiments can be divided into two groups, based on how their mole fractions change when propylene (or propyne) is added, in comparison to those in neat toluene pyrolysis. The first group includes the PAHs that are newly introduced or more abundant in toluene- C_3 co-pyrolysis; the

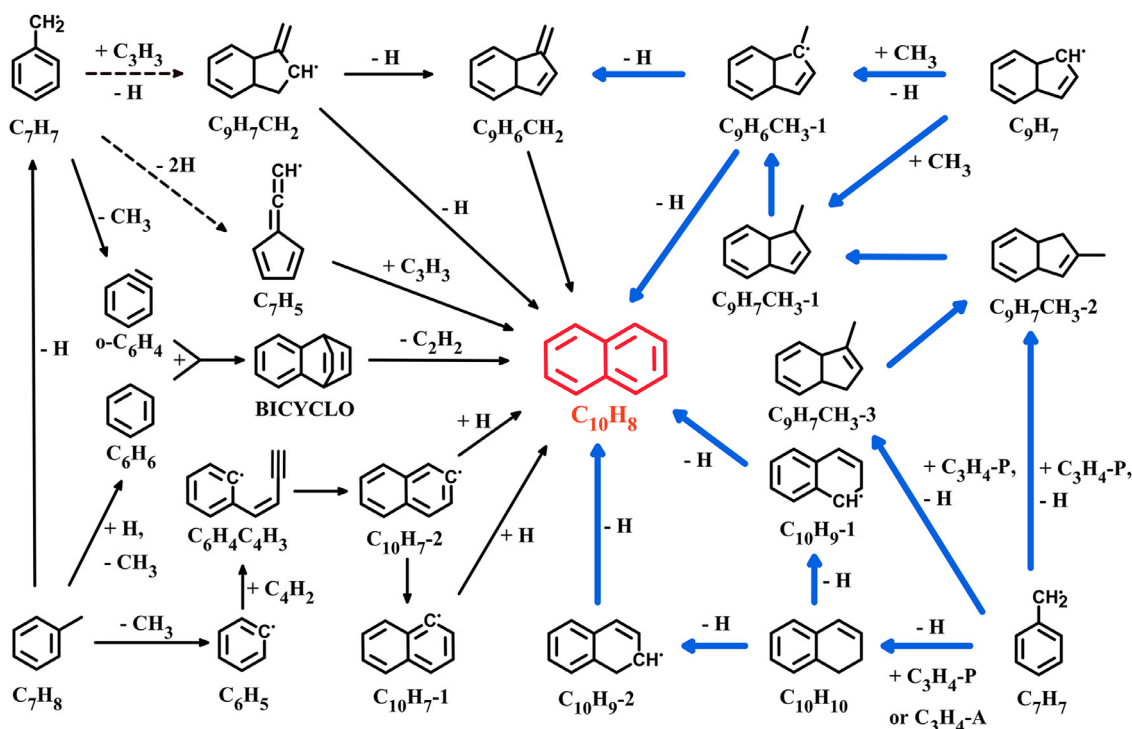


Fig. 10. Naphthalene ($C_{10}H_8$) formation pathways in neat toluene and toluene- C_3 pyrolysis. The highlighted pathways are newly introduced by propylene (or propyne). The dashed arrows indicate that the corresponding pathways are multiple step processes.

PAHs with reduced mole fractions or not clearly influenced by the presence of propylene (or propyne) constitute the second group.

The added C_3 fuels result in a wealth of new PAHs, as can be seen from Fig. 1, and also enhance the concentrations of specific PAHs that already exist in neat toluene pyrolysis. Measured and simulated mole fraction profiles of the first group of PAHs are presented in Fig. 9. To provide a more comprehensive comparison, peak mole fractions of the PAHs measured in neat propylene and propyne pyrolysis [28] under similar conditions are also shown (the initial propylene and propyne concentrations are normalized to the same with those in the current work). To point out, in the following discussion, we mainly address the effects brought by propylene and propyne in comparison to the case of neat toluene pyrolysis. With the addition of propylene (or propyne), indene (C_9H_8) peak mole fractions are brought up to over 5 ppm from less than 1 ppm, and noteworthy, the speciation window shifts to much lower temperatures in toluene-propyne co-pyrolysis. Such observations can be accurately reproduced by the kinetic model. According to the ROP analyzed results at different temperatures, the early C_9H_8 formation originates from the reaction $C_7H_7 + C_3H_4-P = C_9H_8 + CH_3$; when raising the temperature, the $C_7H_7 + C_2H_2$ reactions, directly forming C_9H_8 or via non-PAH isomeric intermediates ($C_6H_5C_3H_3A$ and $C_6H_5C_3H_3P-1$), dominate the production of C_9H_8 . These reactions channels are facilitated by the abundant C_2H_2 formed from C_3 pyrolysis. In toluene-propylene co-pyrolysis, the dehydrogenation of indene (C_9H_{10}) also has a minor contribution to C_9H_8 formation. C_9H_{10} is only observed in toluene-propylene co-pyrolysis with a peak mole fraction below 10^{-7} , and below our detection limit ($\sim 10^{-8}$) in the other two cases. The major formation channel through $C_7H_7 + C_2H_4 = C_9H_{10} + H$ is less efficient than the analogous reaction of $C_7H_7 + C_2H_2$ forming C_9H_8 . Besides, the formed C_9H_{10} mostly undergoes dehydrogenation under the high-pressure pyrolysis conditions.

As anticipated, the extra C_3 fuels, in particular propyne, enhance the naphthalene ($C_{10}H_8$) formation from toluene pyroly-

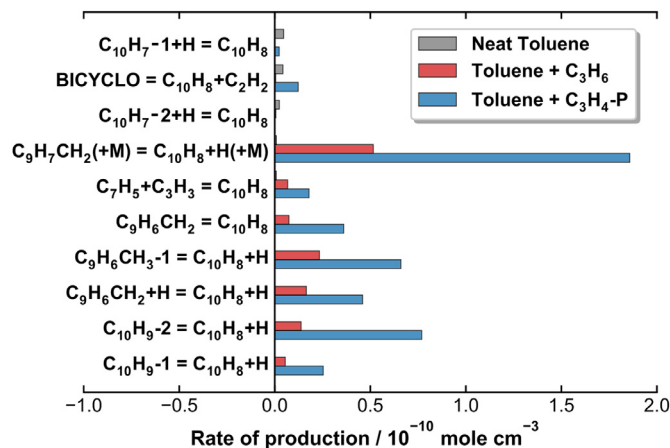


Fig. 11. Integrated ROP coefficients for naphthalene formation over a reaction time of 4 ms in neat toluene pyrolysis, toluene-propylene and toluene-propyne co-pyrolysis at T_5 of 1400 K.

sis to a large extent, and lower the speciation temperature window. Figure 10 displays a reaction scheme centering on the formation of $C_{10}H_8$ from smaller precursors. This scheme is based on the ROP-analyzed results at T_5 of 1400 K in all three studied cases, and the reaction pathways introduced by propylene (or propyne) are highlighted. The more quantitative analyzed results, i.e. the integrated ROP-coefficients of the major $C_{10}H_8$ formation reactions, are presented in Fig. 11. In neat toluene pyrolysis, only a negligible amount of $C_{10}H_8$ is formed at 1400 K, mainly through the naphthyl+H recombination and the fragmentation of benzocyclo[2,2,2]octatriene (BICYCLO) formed from the $C_6H_6 + o$ -benzynes (o - C_6H_4) reaction. Other minor channels include the $C_7H_5 + C_3H_3$ recombination and the decomposition of $C_9H_7CH_2$ produced from the $C_7H_7 + C_3H_3$ reaction, directly or through

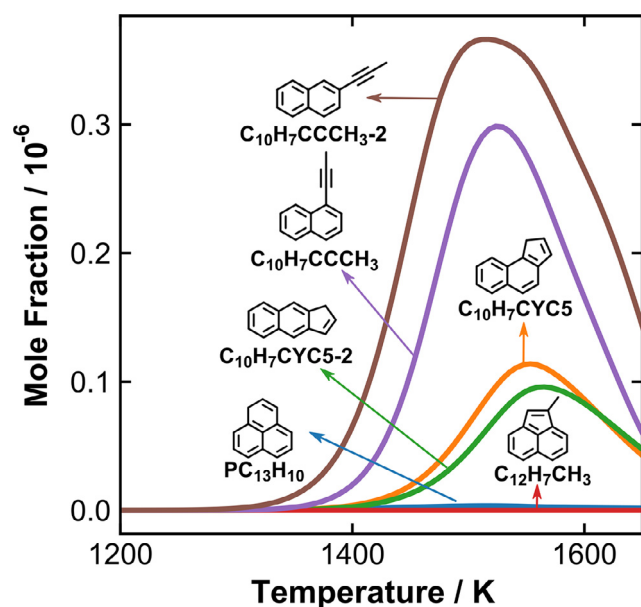


Fig. 12. Simulated mole fraction profiles of $C_{13}H_{10}$ isomers, which are potential products of $C_{10}H_7 + C_3H_3/C_3H_4$ reactions, in toluene-propyne co-pyrolysis.

benzofulvene ($C_9H_6CH_2$) as an intermediates. These minor channels are significantly intensified due to the increased C_3H_3 level in toluene- C_3 co-pyrolysis. Moreover, some newly-introduced channels are found to play a role in $C_{10}H_8$ formation, such as the dehydrogenation/consumption of dihydronaphthalene ($C_{10}H_{10}$) and 1-methylindene ($C_9H_7CH_3-1$). Both $C_{10}H_8$ precursors are already formed through the $C_7H_7 + C_3H_4-P/C_3H_4-A$ reactions at relatively low temperatures below 1400 K, as evidenced by their observation in toluene- C_3 co-pyrolysis experiments (see Fig. 1). As can be noted from Fig. 11, the relevant importance of the major $C_{10}H_8$ formation reactions is similar in toluene-propylene and toluene-propyne co-pyrolysis, though the absolute $C_{10}H_8$ production in the former case is much lower. This is because in both cases, these reactions need the participation of propyne and propargyl, which are more sufficient in toluene-propyne co-pyrolysis. The kinetic model can well capture the increasing trend in $C_{10}H_8$ concentrations when propylene (or propyne) is added. The lowered speciation window is also predicted, but not as pronounced as measured during the experiments. The reaction channels of benzyl addition to propyne play an important role in $C_{10}H_8$ formation at relatively low temperatures. However, relevant reaction processes and rate coefficients are determined through analogies since no theoretically determined kinetic parameters are available. The model prediction performances for naphthalene in toluene-propylene (or propyne) co-pyrolysis can be optimized if the reaction kinetics of $C_7H_7 + C_3H_4-P$ can be refined.

The results for the ROP analyses of $C_{10}H_8$ at a higher temperature of $T_5 = 1500$ K are given in Fig. S4. All mentioned reaction channels have greater contributions to naphthalene formation, and in particular, the dehydrogenation of $C_9H_6CH_3-1$ and the isomerization of $C_9H_6CH_2$ have higher relative importance. This is because the indenyl (C_9H_7)+ $\dot{C}H_3$ channel becomes another major source of $C_9H_7CH_3-1$ besides the above-mentioned $C_7H_7 + C_3H_4-P$ reactions. Therefore, the pathway via $C_9H_7CH_3-1 \rightarrow C_9H_6CH_3-1 \rightarrow C_9H_6CH_2 \rightarrow C_{10}H_8$ is strengthened. The increased indene (C_9H_8) formation gives rise to higher C_9H_7 production in toluene- C_3 co-pyrolysis, where $\dot{C}H_3$ is also abundant. The reaction sequence starting from C_9H_7 methylation leading to naphthalene ($C_{10}H_8$) has been established as a typical pathway converting a five-membered ring to a six-membered ring in PAH growth [41]. The molecu-

lar PAH intermediates, 1- and 2- methyl indene ($C_9H_7CH_3-1$ and $C_9H_7CH_3-2$), which are involved in the reaction PES [41], are separately quantified in the current experiments of toluene- C_3 co-pyrolysis. The measured temperature-dependent mole fractions are provided in Fig. 9(f) and (g), which are however largely underestimated by the kinetic model. This is because the formation of methylindene isomers continues after the arrival of the rarefaction waves, so that the measurements cannot be characterized by the simulations based on the constant pressure assumption over a reaction time of 4 ms. To illustrate this point, the time dependent mole fractions for specific species simulated using the measured pressure history in toluene-propyne pyrolysis at T_5 of 1425 K are provided in Fig. S5. The left column shows the mole fraction profiles of major radicals including $\dot{C}H_3$ and the resonance-stabilized C_3H_3 , C_7H_7 and C_9H_7 , and some species that directly result from the recombination of these radicals, such as ethylbenzene ($C_6H_5C_2H_5$, formed through $C_7H_7 + \dot{C}H_3$), 2,3-butadienylbenzene ($C_6H_5CC^*C$, formed through $C_7H_7 + C_3H_3$), $C_9H_7CH_3-1$ (formed through $C_9H_7 + \dot{C}H_3$) and bibenzyl ($C_6H_5C_2H_4C_6H_5$, formed through $C_7H_7 + C_7H_7$). The formation of these species through radical recombination carries on during the post-shock quenching. The PAHs shown in the right column of Fig. S5 exhibit very different speciation behaviors: their formation completes by the defined reaction time of 4 ms, after which the mole fractions no longer change. By considering the reactions that occur during the post-shock quenching, $C_9H_7CH_3-2$ mole fractions can be well reproduced, while the contents of $C_9H_7CH_3-1$ are still under-estimated. Another methylindene isomer, $C_9H_7CH_3-3$, is considered as a potential product of the $C_7H_7 + C_3H_4-P$ addition-elimination reactions, as mentioned in the modeling section. The model predicts that $C_9H_7CH_3-3$ has comparable abundance with $C_9H_7CH_3-1$ and $C_9H_7CH_3-2$, though it is not identified in the current experiments. The conversion from $C_9H_7CH_3-3$ to $C_9H_7CH_3-1$ is perhaps underestimated in the current model, leading to the aforementioned discrepancies between the observations and simulations. Future theoretical works on the $C_7H_7 + C_3H_4-P$ reactions and the conversion among methylindene isomers are needed, which may benefit better model predictions for the methylindene isomers. Since naphthalene becomes much more abundant in toluene- C_3 co-pyrolysis, the formation of PAHs with substituted naphthalene structures also increases. The isomers 1-methyl-naphthalene ($C_{10}H_7CH_3-1$) and 2-methyl-naphthalene ($C_{10}H_7CH_3-2$) are separately quantified in the current work. In all three studied cases, $C_{10}H_7CH_3-2$ has slightly higher peak mole fractions than $C_{10}H_7CH_3-1$, and this feature can be well reproduced by the kinetic model. For the C_2 substituted naphthalene PAHs, such as vinyl- and ethynyl-naphthalene, not all possible isomers are detected in the experiments due to the unarchived standard mass spectra or potential signal overlaps. For the identified ones (1-ethynyl-naphthalene and 1-vinylnaphthalene), the kinetic model can satisfactorily predict the measurements and the right order of the peak mole fractions among the three cases.

The mole fractions of acenaphthalene ($C_{12}H_8$) increase remarkably when propylene (or propyne) is added. Besides, the onset temperature of $C_{12}H_8$ formation is brought down to about 1300 K in toluene-propyne co-pyrolysis. ROP analyzed results at T_5 of 1500 K indicate that two major pathways account for the formation of $C_{12}H_8$ in neat toluene pyrolysis: the step-wise isomerization via biphenylene ($C_6H_4C_6H_4$) and cyclopenta[a]indene (BENZO) as intermediates on a $C_{12}H_9$ reaction PES [47,48] and a reaction pathway starting from $C_9H_7 + C_3H_3$ recombination [49], as discussed in our previous work [12]. The latter channel becomes exclusively dominant (over 90%) in toluene- C_3 co-pyrolysis due to the sufficient production of C_9H_7 and C_3H_3 . In all studied cases, the Hydrogen Abstraction- C_2H_2 -Addition (HACA) route via $C_{10}H_7-1 + C_2H_2$ only has a limited contribution (a few

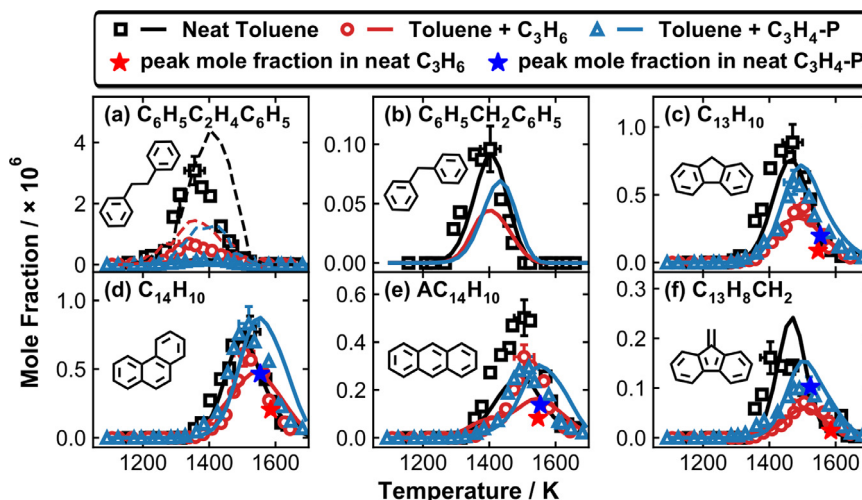


Fig. 13. Measured (symbols) and simulated (solid lines) mole fractions of the second group of PAH species in neat toluene, toluene + C_3H_6 and toluene + C_3H_4 -P pyrolysis. For $C_6H_5C_2H_4C_6H_5$, whose mole fractions are significantly influenced by the reactions during the quenching period, simulated mole fractions using the measured pressure profiles up to 10 ms (dashed lines) are also presented. Measured PAH peak mole fractions in neat propylene and propyne pyrolysis come from [28], with initial C_3 fuel concentrations being normalized to the same with those in toluene-propylene (or propyne) pyrolysis.

percent) at T_5 of 1500 K, though its importance increases at elevated temperatures.

Similar to the fact that the significant increase in $C_{12}H_8$ formation arises from the increased indene (C_9H_8) production and the abundant C_3 species in toluene- C_3 co-pyrolysis, it is anticipated that the enhanced naphthalene ($C_{10}H_8$) formation would result in abundant C_{13} PAHs through $C_{10}+C_3$ reactions, particularly in toluene-propyne co-pyrolysis. The reactions between naphthyl ($C_{10}H_7-1$ and $C_{10}H_7-2$) and C_3 species are considered in the kinetic model based on literature theoretical works [38–40] and analogies to $C_6H_5+C_3H_x$ reactions. A few $C_{13}H_{10}$ species are identified in the current experiments (the small peaks with the retention time of 9.5 min, see Fig. 1), but the exact structures cannot be specified due to their trace amounts and the absence of standard mass spectra. Figure 12 displays the simulated mole fractions of $C_{13}H_{10}$ isomers that potentially come from $C_{10}+C_3$ reactions (see Scheme 1): the 1-naphthyl-propyne isomers ($C_{10}H_7CCCH_3$ and $C_{10}H_7CCCH_3-2$) are predicted to be the major $C_{13}H_{10}$ products; regarding the three-ring PAH isomers, only 1H-benz[e]indene ($C_{10}H_7CYC5$) and 1H-benz[f]indene ($C_{10}H_7CYC5-2$) have peak mole fractions around 10^{-7} , while the amounts of phenalene ($PC_{13}H_{10}$) and 1-methylacenaphthalene ($C_{12}H_7CH_3$) are negligible. Different from the abundant indenyl which is resonance-stabilized, naphthyl radicals have relatively low (at the level of 10^{-8}) concentrations even in toluene-propyne co-pyrolysis. Consequently, $C_{10}H_7+C_3$ reactions are not efficient pathways leading to PAH growth as the recombination reactions of resonance-stabilized radicals, such as $C_7H_7+C_3H_3$ and $C_9H_7+C_3H_3$ leading to $C_{10}H_8$ and $C_{12}H_8$, respectively. The relevant $C_{13}H_{10}$ PAHs are therefore of limited abundance in toluene-propyne pyrolysis, in spite of the largely increased $C_{10}H_8$ formation and the plentiful C_3H_3 .

In all three cases, the formation of biphenyl ($C_6H_5C_6H_5$) relies on the reaction $C_6H_6+C_6H_5 = C_6H_5C_6H_5+H$, and the hydrogen abstraction from C_6H_6 is an important source of C_6H_5 . Thus, the peak mole fractions of $C_6H_5C_6H_5$ follow the same order with those of C_6H_6 among the three cases. Diphenylacetylene ($C_6H_5CCC_6H_5$) mainly comes from the reactions between $C_6H_5C_2H_2$ and C_6H_5 , so the addition of propylene (or propyne) enhances the production of $C_6H_5CCC_6H_5$ by facilitating the production of both precursors.

The PAHs included in the second group are all C_{13} – C_{14} species, for which the measured and simulated mole fraction profiles are

shown in Fig. 13. Biphenyl ($C_6H_5C_2H_4C_6H_5$) is measured to be the most abundant PAH in neat toluene pyrolysis, and as mentioned above, a significant portion of $C_6H_5C_2H_4C_6H_5$ is actually produced via C_7H_7 self-recombination during the post-shock quenching (see Fig. S5). The use of the measured pressure profiles up to 10 ms is therefore necessary to simulate the mole fractions of $C_6H_5C_2H_4C_6H_5$. Despite an over-prediction for the absolute mole fractions, the model can capture the observation that $C_6H_5C_2H_4C_6H_5$ mole fractions largely decline when propylene or propyne is added to toluene pyrolysis. This derives from the fact that the C_7H_7 self-recombination is impeded by the competing reactions of C_7H_7 with the abundant C_1 – C_3 species in toluene- C_3 co-pyrolysis. Propyne brings about more obvious inhibiting effects on $C_6H_5C_2H_4C_6H_5$ formation than propylene, since the direct reactions with propyne are identified as important consumption channels of C_7H_7 in toluene-propyne co-pyrolysis (see Fig. 5). Biphenylmethane ($C_6H_5CH_2C_6H_5$) mole fractions cannot be accurately quantified in toluene- C_3 co-pyrolysis, because the GC signal peak of $C_6H_5CH_2C_6H_5$ overlaps with that of $C_{10}H_7C_2H_3$, and the latter has much (about 10 times) higher mole fractions according to the model predictions. The kinetic model can well capture the mole fraction distribution of $C_6H_5CH_2C_6H_5$ in neat toluene pyrolysis, and it predicts that $C_6H_5CH_2C_6H_5$ has lower mole fractions in toluene- C_3 co-pyrolysis. The reason lies in that a reduced portion of C_7H_7 participates the $C_7H_7+C_6H_5$ recombination leading to $C_6H_5CH_2C_6H_5$. On the other hand, the other $C_6H_5CH_2C_6H_5$ precursor, C_6H_5 , has higher abundance when the C_3 fuels are added, particularly in toluene-propyne co-pyrolysis, where the $C_6H_5CH_2C_6H_5$ peak mole fraction is therefore only slightly affected. Fluorene ($FC_{13}H_{10}$), which comes from $C_6H_5CH_2C_6H_5$ dehydrogenation reactions, is one of the major PAHs observed in neat toluene pyrolysis. The peak mole fractions of $FC_{13}H_{10}$ are lower in toluene- C_3 co-pyrolysis, as a consequence of the reduced production of the precursor $C_6H_5CH_2C_6H_5$. Nevertheless, in comparison to the above-mentioned $C_{13}H_{10}$ species formed via $C_{10}+C_3$ reactions, $FC_{13}H_{10}$ is still the most abundant $C_{13}H_{10}$ isomer.

Phenanthrene ($PC_{14}H_{10}$) is observed of similar peak mole fractions in all three cases, only slightly less in toluene-propylene co-pyrolysis, and such phenomena can be reproduced by the kinetic model. The model predicts a similar trend for the peak mole fractions of anthracene ($AC_{14}H_{10}$), the other three-aromatic-ring isomer, among the three cases, though $AC_{14}H_{10}$ is measured of higher

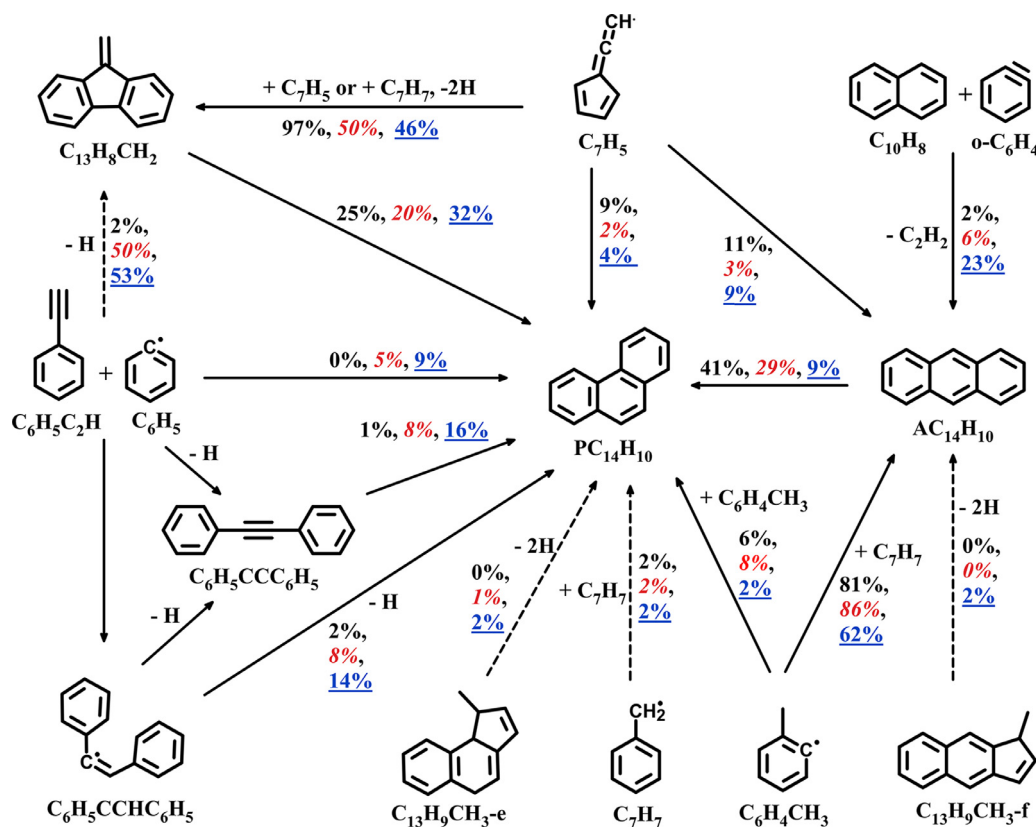


Fig. 14. Formation pathways for $PC_{14}H_{10}$ and $AC_{14}H_{10}$ in the pyrolysis of neat toluene and toluene-propylene and toluene-propyne mixtures at T_5 of 1500 K. The percentage numbers (normal: neat toluene; italic: toluene+propylene; underlined: toluene+propyne) represent the contributions of corresponding reactions to the formation of $C_{14}H_{10}$ PAHs. The dashed lines represent multiple step reaction processes.

concentrations in neat toluene pyrolysis. Reaction pathways leading to the formation of $PC_{14}H_{10}$ and $AC_{14}H_{10}$ based on ROP analysis at T_5 of 1500 K are shown Fig. 14. A general trend is that the C_7+C_7 ($C_7H_7+C_7H_7$, $C_7H_5+C_7H_5$, $C_7H_7+C_7H_5$, $C_6H_4CH_3+C_6H_4CH_3$ and $C_7H_7+C_6H_4CH_3$) reactions have decreased importance when propylene (or propyne) is added to toluene pyrolysis. This is due to the fact that the C_7 radicals have lower concentrations after reacting with the C_3 and smaller species. 9-methylene-fluorene ($C_{13}H_8CH_2$) is recognized as an important precursor of $PC_{14}H_{10}$. When propylene (or propyne) is added to neat toluene pyrolysis, the speciation of $C_{13}H_8CH_2$ shifts to higher temperature windows and the peak mole fractions decrease (see Fig. 13(f)). Such features can be captured by the kinetic model. In neat toluene pyrolysis, $C_{13}H_8CH_2$ is mainly formed through $C_7H_7+C_7H_5 \Rightarrow C_{13}H_8CH_2+2H$, analogous to the $C_3H_5-A+C_3H_3$ reaction forming fulvene. This channel is hindered in toluene- C_3 co-pyrolysis, resulting in reduced $C_{13}H_8CH_2$ mole fractions, though $C_{13}H_8CH_2$ is formed via an alternative pathway, the addition-elimination reaction of $C_6H_5C_2H+C_6H_5$. $C_6H_5C_2H$ starts to produce at relatively high temperatures and the production of $C_6H_5C_2H$ is enhanced when C_3 , especially propyne, is introduced to the reaction system of toluene pyrolysis (see Fig. 7(b)). These factors rationalize that the peak mole fractions of $C_{13}H_8CH_2$ appear at higher temperatures in toluene- C_3 co-pyrolysis, compared to that in neat toluene pyrolysis, and that $C_{13}H_8CH_2$ is more abundant in toluene-propyne co-pyrolysis than in toluene-propylene co-pyrolysis. The reaction scheme for the formation of $AC_{14}H_{10}$ is less understood than that of $PC_{14}H_{10}$. According to the current model, $AC_{14}H_{10}$ is mainly from the reaction between C_7H_7 and $CH_3C_6H_4$ in all three reaction systems. This channel is inhibited when C_3 fuel is added, while the π -bonding process of naphthalene ($C_{10}H_8$)+ o -benzynes ($o-C_6H_4$) has an increasing contribution, owing to the higher abun-

dance of $C_{10}H_8$. The newly included channel through the dehydrogenation and ring-rearrangements of $C_{13}H_9CH_3-f$ (see Scheme 1) results in a negligible amount of $AC_{14}H_{10}$, because of the limited level of $C_{10}H_7CYC-2$ (see Fig. 12), the precursor of $C_{13}H_9CH_3-f$. Sensitivity analysis for $AC_{14}H_{10}$ at T_5 of 1500 K is performed and the results are shown in Fig. S6. The lumped reaction $C_7H_7+CH_3C_6H_4 \Rightarrow H_2+2H+AC_{14}H_{10}$ has the highest sensitivity coefficients facilitating $AC_{14}H_{10}$ formation, and the conversion to $PC_{14}H_{10}$ is a dominant process reducing $AC_{14}H_{10}$ mole fractions. The hydrogen abstraction reactions by H (in all three cases) and by $\dot{C}H_3$ (in toluene- C_3 co-pyrolysis) forming $CH_3C_6H_4$ also have relatively high positive sensitive coefficients, indicating that the formation of $AC_{14}H_{10}$ is highly relevant to the chemistry of $CH_3C_6H_4$, which is however not as well established as that of C_7H_7 . Besides, there might be other $AC_{14}H_{10}$ formation reactions missing from the current kinetic model. Future works on $CH_3C_6H_4$ reactions, for instance the recombination with C_7H_7 , and other possible channels leading to $AC_{14}H_{10}$ are highly necessary.

5. Conclusions

Co-pyrolysis of toluene and propylene (or propyne), is studied in this work through shock tube experiments and detailed kinetic modeling over a temperature range of 1050–1700 K and at a nominal pressure of 20 bar. By taking neat toluene pyrolysis as a reference, the influences of the propyne/propylene addition on fuel reactivity and speciation behaviors are discussed. The consumption of propyne/propylene via the reaction $C_3H_x+H = C_2H_{x-2}+\dot{C}H_3$ ($x = 6, 4$) results in abundant CH_3 , and thus facilitates toluene consumption through hydrogen abstraction reactions by CH_3 . However, propylene and propyne also compete with toluene for radical consumption, so overall, the decomposition reactivity of toluene is

not significantly affected by the addition of propyne and propylene. Different from the “synergistic effects” observed in toluene-C₂ co-pyrolysis, the decomposition reactivity of propylene and propyne is not apparently changed by the presence of toluene. The levels of C₁–C₃ species are much higher in toluene-C₃ co-pyrolysis than in neat toluene pyrolysis, and the interactions between the small species and the aromatics, particularly benzyl, bring about new species, and alter the distribution of carbon flux from toluene/benzyl to different pyrolysis products. The addition of propylene (or propyne) promotes the formation of benzene, mainly through propargyl self-recombination, and consequently, more diverse and abundant MAHs are observed in toluene-C₃ co-pyrolysis. New types of PAHs are identified when the studied C₃ fuels are added to toluene pyrolysis, in particular C₁₀ species which are direct evidence of the interactions between toluene/benzyl and C₃ species. C₃H₄-P and C₃H₃ play an essential role in such interactions, which accounts for the fact that the addition of propyne, compared to propylene, induces more obvious effects. Increases are seen in the mole fractions of the PAHs whose formation depends on the reactions involving C₁–C₃ species. The enhanced indene mole fractions come from the direct yield from C₇H₇+C₃H₄-P and C₇H₇+C₂H₂ reactions. The formation of acenaphthalene via the C₉H₇+C₃H₃ reaction sequence is facilitated by the sufficient production of both precursors. Naphthalene is found as the most abundant PAH in toluene-C₃ co-pyrolysis, with a peak mole fraction over 10 ppm in toluene-propyne co-pyrolysis. The reasons are threefold: the formation channel through the C₇H₇+C₃H₃ reactions is significantly strengthened; the interactions between C₇H₇ and C₃H₄-P/C₃H₄-A result in dihydronaphthalene, which further undergoes dehydrogenation to form naphthalene; 1-methylindene becomes an important naphthalene precursor, due to the intensified C₉H₇+CH₃ channel and the conversion of other methylindene isomers resulting from the C₇H₇+C₃H₄-P reactions. The level of C₇ radicals are reduced due to their reactions with C₁–C₃ species. Therefore the PAHs which largely rely on C₇+C₇ reactions, such as bibenzyl and the three-ring aromatics phenanthrene and anthracene, show decreasing trends in their mole fractions in toluene-C₃ co-pyrolysis.

Declaration of Competing Interest

The authors declare that they have no known competing financial interests or personal relationships that could have appeared to influence the work reported in this paper.

Acknowledgments

This project has received funding from the [European Research Council](#) (ERC) under the European Union's Horizon 2020 research and innovation program (grant agreement No. [756785](#)).

Supplementary materials

Supplementary material associated with this article can be found, in the online version, at doi:[10.1016/j.combustflame.2021.111799](#).

References

- [1] R.D. Smith, A direct mass spectrometric study of the mechanism of toluene pyrolysis at high temperatures, *J. Phys. Chem.* 83 (1979) 1553–1563.
- [2] K. Pamidimukkala, R. Kern, M. Patel, H. Wei, J. Kiefer, High-temperature pyrolysis of toluene, *J. Phys. Chem.* 91 (1987) 2148–2154.
- [3] M. Braun-Unkhoff, P. Frank, T. Just, A shock tube study on the thermal decomposition of toluene and of the phenyl radical at high temperatures, *Proc. Combust. Inst.* 22 (1989) 1053–1061.
- [4] M. Colket, D. Seery, Reaction mechanisms for toluene pyrolysis, *Proc. Combust. Inst.* 25 (1994) 883–891.
- [5] R. Sivaramakrishnan, R.S. Tranter, K. Brezinsky, High pressure pyrolysis of toluene. 1. Experiments and modeling of toluene decomposition, *J. Phys. Chem. A* 110 (2006) 9388–9399.
- [6] S.J. Klippenstein, L.B. Harding, Y. Georgievskii, On the formation and decomposition of C₇H₈, *Proc. Combust. Inst.* 31 (2007) 221–229.
- [7] B. Shukla, A. Susa, A. Miyoshi, M. Koshi, In situ direct sampling mass spectrometric study on formation of polycyclic aromatic hydrocarbons in toluene pyrolysis, *J. Phys. Chem. A* 111 (2007) 8308–8324.
- [8] T. Zhang, L. Zhang, X. Hong, K. Zhang, F. Qi, C.K. Law, T. Ye, P. Zhao, Y. Chen, An experimental and theoretical study of toluene pyrolysis with tunable synchrotron VUV photoionization and molecular-beam mass spectrometry, *Combust. Flame* 156 (2009) 2071–2083.
- [9] L. Zhang, J. Cai, T. Zhang, F. Qi, Kinetic modeling study of toluene pyrolysis at low pressure, *Combust. Flame* 157 (2010) 1686–1697.
- [10] A. Matsugi, A. Miyoshi, Modeling of two- and three-ring aromatics formation in the pyrolysis of toluene, *Proc. Combust. Inst.* 34 (2013) 269–277.
- [11] W. Yuan, Y. Li, P. Dagaut, J. Yang, F. Qi, Investigation on the pyrolysis and oxidation of toluene over a wide range conditions. I. Flow reactor pyrolysis and jet stirred reactor oxidation, *Combust. Flame* 162 (2015) 3–21.
- [12] W. Sun, A. Hamadi, S. Abid, N. Chaumeix, A. Comandini, Probing PAH formation chemical kinetics from benzene and toluene pyrolysis in a single-pulse shock tube, *Proc. Combust. Inst.* 38 (2021) 891–900.
- [13] D. Astholz, J. Durant, J. Troe, Thermal decomposition of toluene and of benzyl radicals in shock waves, *Proc. Combust. Inst.* 18 (1981) 885–892.
- [14] V.S. Rao, G.B. Skinner, Formation of hydrogen atoms in pyrolysis of ethylbenzene behind shock waves. Rate constants for the thermal dissociation of the benzyl radical, *Proc. Combust. Inst.* 21 (1988) 809–814.
- [15] J. Jones, G.B. Bacskay, J.C. Mackie, Decomposition of the benzyl radical: quantum chemical and experimental (shock tube) investigations of reaction pathways, *J. Phys. Chem. A* 101 (1997) 7105–7113.
- [16] C. Cavallotti, M. Derudi, R. Rota, On the mechanism of decomposition of the benzyl radical, *Proc. Combust. Inst.* 32 (2009) 115–121.
- [17] G. da Silva, J.A. Cole, J.W. Bozzelli, Thermal decomposition of the benzyl radical to fulvalene (C₇H₆) + H, *J. Phys. Chem. A* 113 (2009) 6111–6120.
- [18] D. Polino, M. Parrinello, Combustion chemistry via metadynamics: benzyl decomposition revisited, *J. Phys. Chem. A* 119 (2015) 978–989.
- [19] A. Matsugi, Thermal decomposition of benzyl radicals: kinetics and spectroscopy in a shock tube, *J. Phys. Chem. A* 124 (2020) 824–835.
- [20] L. Vereecken, J. Peeters, Reactions of chemically activated C₉H₉ species II: the reaction of phenyl radicals with allene and cyclopropene, and of benzyl radicals with acetylene, *Phys. Chem. Chem. Phys.* 5 (2003) 2807–2817.
- [21] A.M. Mebel, Y. Georgievskii, A.W. Jasper, S.J. Klippenstein, Pressure-dependent rate constants for PAH growth: formation of indene and its conversion to naphthalene, *Faraday Discuss.* 195 (2017) 637–670.
- [22] W. Sun, A. Hamadi, S. Abid, N. Chaumeix, A. Comandini, Detailed experimental and kinetic modeling study of toluene/C₂ pyrolysis in a single-pulse shock tube, *Combust. Flame* 226 (2021) 129–142.
- [23] N. Marinov, W. Pitz, C. Westbrook, A. Lutz, A. Vincitore, S. Senkan, Chemical kinetic modeling of a methane opposed-flow diffusion flame and comparison to experiments, *Proc. Combust. Inst.* 27 (1998) 605–613.
- [24] A. Matsugi, A. Miyoshi, Computational study on the recombination reaction between benzyl and propargyl radicals, *Int. J. Chem. Kinet.* 44 (2012) 206–218.
- [25] A. Matsugi, A. Miyoshi, Reactions of o-benzyne with propargyl and benzyl radicals: potential sources of polycyclic aromatic hydrocarbons in combustion, *Phys. Chem. Chem. Phys.* 14 (2012) 9722–9728.
- [26] S. Sinha, A. Raj, Polycyclic aromatic hydrocarbon (PAH) formation from benzyl radicals: a reaction kinetics study, *Phys. Chem. Chem. Phys.* 18 (2016) 8120–8131.
- [27] S. Sinha, R.K. Rahman, A. Raj, On the role of resonantly stabilized radicals in polycyclic aromatic hydrocarbon (PAH) formation: pyrene and fluoranthene formation from benzyl–indenyl addition, *Phys. Chem. Chem. Phys.* 19 (2017) 19262–19278.
- [28] W. Sun, A. Hamadi, S. Abid, N. Chaumeix, A. Comandini, A comprehensive kinetic study on the speciation from propylene and propyne pyrolysis in a single-pulse shock tube, *Combust. Flame* 231 (2021) 11485.
- [29] W. Sun, A. Hamadi, S. Abid, N. Chaumeix, A. Comandini, An experimental and kinetic modeling study of phenylacetylene decomposition and the reactions with acetylene/ethylene under shock tube pyrolysis conditions, *Combust. Flame* 220 (2020) 257–271.
- [30] W. Sun, A. Hamadi, S. Abid, N. Chaumeix, A. Comandini, A comparative kinetic study of C₈–C₁₀ linear alkylbenzenes pyrolysis in a single-pulse shock tube, *Combust. Flame* 221 (2020) 136–149.
- [31] T. Li, Y. Zhang, W. Yuan, C. Cao, W. Li, J. Yang, Y. Li, Unraveling synergistic effects on pyrolysis reactivity and indene formation in co-pyrolysis of toluene and acetylene, *Proc. Combust. Inst.* 38 (2020) 1413–1421.
- [32] K. Wang, S.M. Villano, A.M. Dean, Fundamentally-based kinetic model for propene pyrolysis, *Combust. Flame* 162 (2015) 4456–4470.
- [33] A.N. Morozov, A.M. Mebel, Theoretical study of the reaction mechanism and kinetics of the phenyl+ propargyl association, *Phys. Chem. Chem. Phys.* 22 (2020) 6868–6880.
- [34] A.N. Morozov, A.M. Mebel, Theoretical study of the reaction mechanism and kinetics of the phenyl+ allyl and related benzyl+ vinyl associations, *J. Phys. Chem. A* 123 (2019) 1720–1729.
- [35] W. Pejpichestakul, E. Ranzi, M. Pelucchi, A. Frassoldati, A. Cuoci, A. Parente, T. Faravelli, Examination of a soot model in premixed laminar flames at fuel-rich conditions, *Proc. Combust. Inst.* 37 (2019) 1013–1021.

- [36] A. Semnikhin, A. Savchenkova, I. Chechet, S. Matveev, Z. Liu, M. Frenklach, A. Mebel, Rate constants for H abstraction from benzo (a) pyrene and chrysene: a theoretical study, *Phys. Chem. Chem. Phys.* 19 (2017) 25401–25413.
- [37] A. Laskin, C. Tamburu, F. Dubnikova, A. Lifshitz, Production of major reaction products in the initial steps of the thermal decomposition of naphthalene. Experimental shock-tube results and computer simulation, *Proc. Combust. Inst.* 35 (2015) 299–307.
- [38] A. Raj, M.J. Al Rashidi, S.H. Chung, S.M. Sarathy, PAH growth initiated by propargyl addition: mechanism development and computational kinetics, *J. Phys. Chem. A* 118 (2014) 2865–2885.
- [39] D.P. Porfiriev, V.N. Azyazov, A.M. Mebel, Conversion of acenaphthalene to phenalene via methylation: a theoretical study, *Combust. Flame* 213 (2020) 302–313.
- [40] L. Zhao, R.I. Kaiser, W. Lu, M. Ahmed, A.D. Oleinikov, V.N. Azyazov, A.M. Mebel, A.H. Howlader, S.F. Wnuk, Gas phase formation of phenalene via 10π -aromatic, resonantly stabilized free radical intermediates, *Phys. Chem. Chem. Phys.* 22 (2020) 15381–15388.
- [41] L. Zhao, R.I. Kaiser, W. Lu, B. Xu, M. Ahmed, A.N. Morozov, A.M. Mebel, A.H. Howlader, S.F. Wnuk, Molecular mass growth through ring expansion in polycyclic aromatic hydrocarbons via radical–radical reactions, *Nat. Commun.* 10 (2019) 1–7.
- [42] E.R. Ritter, J.W. Bozzelli, THERM: thermodynamic property estimation for gas phase radicals and molecules, *Int. J. Chem. Kinet.* 23 (1991) 767–778.
- [43] S. Burke, J. Simmie, H. Curran, Critical evaluation of thermochemical properties of C1–C4 species: updated group-contributions to estimate thermochemical properties, *J. Phys. Chem. Ref. Data* 44 (2015) 013101.
- [44] COSILABThe Combustion Simulation Laboratory, Rotexo GmbH & Co., KG, Haan, Germany, 2009 Version 3.3.2.
- [45] W. Tang, K. Brezinsky, Chemical kinetic simulations behind reflected shock waves, *Int. J. Chem. Kinet.* 38 (2006) 75–97.
- [46] X. Han, J.M. Mehta, K. Brezinsky, Temperature approximations in chemical kinetics studies using single pulse shock tubes, *Combust. Flame* 209 (2019) 1–12.
- [47] B. Shukla, K. Tsuchiya, M. Koshi, Novel products from C₆H₅+ C₆H₆/C₆H₅ reactions, *J. Phys. Chem. A* 115 (2011) 5284–5293.
- [48] A. Comandini, T. Malewicki, K. Brezinsky, Chemistry of polycyclic aromatic hydrocarbons formation from phenyl radical pyrolysis and reaction of phenyl and acetylene, *J. Phys. Chem. A* 116 (2012) 2409–2434.
- [49] H. Jin, L. Xing, J. Hao, J. Yang, Y. Zhang, C. Cao, Y. Pan, A. Farooq, A chemical kinetic modeling study of indene pyrolysis, *Combust. Flame* 206 (2019) 1–20.